

A Joint Experimental and Computational Study on the Electronic Communication in Diethynylaryl-Bridged $(\eta^5\text{-C}_5\text{H}_5)\text{Fe}(\eta^2\text{-dppe})$ and $(\eta^5\text{-C}_5\text{H}_5)\text{-Fe}(\text{CO})_2$ Units

Laura Medei,^[a] Laura Orian,^[b] Oleg V. Semeikin,^[c] Mikhail G. Peterleitner,^[c] Nikolai A. Ustynyuk,^[c] Saverio Santi,^{*,[b]} Christian Durante,^[b] Antonella Ricci,^[d] and Claudio Lo Sterzo^{*,[d]}

Keywords: Mixed-valence compounds / Iron / Electron transfer / Electronic communication / Ethynylaryl bridging ligand

A family of bimetallic complexes $[\text{Cp}(\text{CO})_2\text{Fe-C}\equiv\text{C-Ar-C}\equiv\text{C-Fe}(\text{CO})_2\text{Cp}]$ $\{\text{Cp} = \text{C}_5\text{H}_5; \mathbf{6a-g}: \text{Ar} = \text{C}_4\text{H}_2\text{S} (\mathbf{a}), 3\text{-(C}_4\text{H}_9\text{)-C}_4\text{HS} (\mathbf{b}), 3\text{-(C}_{16}\text{H}_{33}\text{)-C}_4\text{HS} (\mathbf{c}), \text{C}_6\text{H}_4 (\mathbf{d}), 2,5\text{-bis-(OC}_4\text{H}_9\text{)-C}_6\text{H}_2 (\mathbf{e}), 2,5\text{-bis(OC}_8\text{H}_{17}\text{)-C}_6\text{H}_2 (\mathbf{f}), (\text{C}_6\text{H}_4)_2 (\mathbf{g})\}$ was prepared by the three-step Pd-catalysed *extended one-pot* (EOP) synthetic protocol from $\text{Bu}_3\text{Sn-C}\equiv\text{CH}$, X-Ar-X ($\text{X} = \text{I, Br}$) and $\text{Cp}(\text{CO})_2\text{FeI}$. Complexes $\mathbf{6a,d,g}$ were then exposed to ultraviolet irradiation in the presence of an equivalent amount of 1,2-bis(diphenylphosphanyl)ethane (dppe) to form the corresponding bimetallic complexes $[\text{Cp}(\text{dppe})\text{Fe-C}\equiv\text{C-Ar-C}\equiv\text{C-Fe}(\text{dppe})\text{Cp}]$ ($\mathbf{7a,d,g}$). Compounds $\mathbf{6a-g}$ and $\mathbf{7a,d,g}$ were characterised by cyclic voltammetry (CV). The most significant electrochemical information comes from the oxidation of the dppe derivatives. The ΔE° separations between the subsequent reversible waves suggest that the efficiency of the metal-metal electronic coupling decreases in the order $\mathbf{7a} > \mathbf{7d} > \mathbf{7g}$. Complexes $\mathbf{7a}$ and $\mathbf{7g}$ were also chemically

oxidised with $[\text{Fe}(\text{Cp}^*)]_2[\text{BF}_4]$ $\{\text{Cp}^* = \text{C}_5(\text{CH}_3)_5\}$ and $[\text{Fe}(\text{Cp})]_2[\text{BF}_4]$ respectively, and the near infrared (NIR) spectra of the mixed-valence species $\mathbf{7a}^+$ and $\mathbf{7g}^+$ were recorded. A strong intervalence transition (IT) band was observed only for the radical cation $\mathbf{7a}^+$. While this finding confirms the existence of an electronic interaction between the two termini when a 2,5-thiophene group is present in the spacer, the NIR spectrum of $\mathbf{7g}^+$ reveals a reduced efficiency in conveying electrons when the $\text{C}_4\text{H}_2\text{S}$ moiety is replaced by a 4,4'-biphenyl. In order to rationalise and quantify the extent of electronic communication, ruled by geometrical and electronic factors, density functional computational results on selected $[\text{Cp}(\text{PH}_3)_2\text{Fe}]$ and $[\text{Cp}(\text{CO})_2\text{Fe}]$ binuclear model complexes are reported.

(© Wiley-VCH Verlag GmbH & Co. KGaA, 69451 Weinheim, Germany, 2006)

Introduction

Highly ethynylated organic or organometallic compounds are currently providing new opportunities in projecting materials to be used in electronics, optics and ceramics.^[1]

The attention devoted to such compounds arises from unique chemical and physical properties due to *facile* elec-

tron transfer along rod-like unsaturated molecular chains (eventually) incorporating metal centres.^[2] The possibilities of extended delocalisation through the π networks can hardly influence physical properties such as polarisability, conductivity, and so forth, making these complexes suitable as active components in optoelectronic devices.^[3]

We have recently disclosed a new one-pot route to poly(acetylide)s and poly(metallaacetylide)s based on palladium-catalysed carbon-carbon and metal-carbon bond formation (Scheme 1).^[4]

By this procedure, named *extended one-pot* (EOP), a great variety of organic co- and homopolymers can be straightforwardly obtained with few steps and very good yields, with no need to isolate intermediate compounds (see path a₁ and path b in Scheme 1). Moreover, taking advantage of a new performance of Pd catalysts we discovered, allowing the formation of metal-carbon bonds, also organometallic oligomers and polymers can be conveniently accessed by this procedure^[4a,4b,5] (path a₂ in Scheme 1).

With such versatile synthetic methodology at our disposal, we pursued our study by aiming for the valuation of the electrochemical and optical properties of some spacers

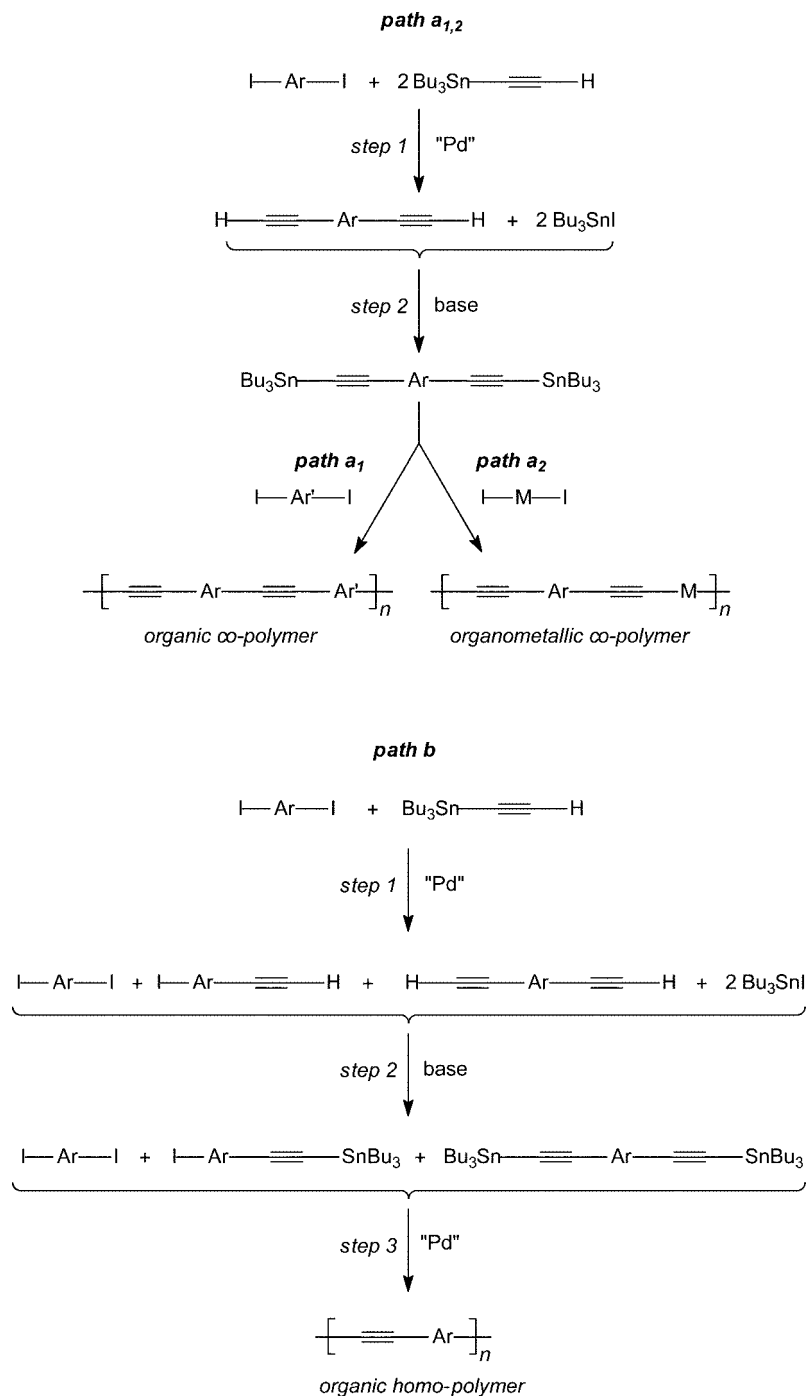
[a] Istituto CNR di Metodologie Chimiche (IMC-CNR), Sezione Meccanismi di Reazione Dipartimento di Chimica, Box 34, Roma 62, Università "La Sapienza", Piazzale Aldo Moro 5, 00185 Roma, Italy

[b] Dipartimento di Scienze Chimiche, Università degli Studi di Padova, Via Marzolo 1, 35131 Padova, Italy
E-mail: saverio.santi@unipd.it

[c] A. N. Nesmeyanov Institute of Organoelement Compounds (INEOS), Russian Academy of Science, Vavilov Street 28, Moscow 119991, Russian Federation

[d] Dipartimento di Scienze degli Alimenti, Facoltà di Agraria, Università degli Studi di Teramo, Via Carlo R. Lerici 1, 64023 Mosciano Sant'Angelo (Teramo), Italy
E-mail: closterzo@unite.it

Supporting information for this article is available on the WWW under <http://www.eurjic.org> or from the author.



Scheme 1.

commonly used as building blocks in the preparation of opto- and electroactive polymers. To achieve this purpose, insertion of different spacers between two iron centres [CpFe(dppe)-] was planned, in order to exploit the electronic interaction between the metallic nuclei in a given redox state and the bridging ligand.

Actually, depending on both the redox state of the molecule and its structure, electron transfer and magnetic exchange can occur along the intermetallic bridge.

Several compounds with different metallic termini, that is iron and rhenium, bridged by unsaturated all-carbon chains (C₄ to C₂₀),^[6a–6j] or iron, ruthenium and osmium, bridged by σ -acetylides intercalated by different aryl cores,^[6k–6m] have been prepared and evaluated for their physical properties by other authors. Elegant studies on the possibility of tuning the electronic communication by lengthening the polyalkynyl bridging ligand and/or by changing the metallic termini have been presented by

Lapinte,^[7] Gladysz^[8] and Bruce^[9] and their co-workers. In a few cases aryl cores have been intercalated in the hydrocarbon spacer.^[7g,7h,7k,7l,7o,7p,7s]

In this paper new binuclear Fe^{II} compounds incorporating aromatic groups are presented. Aromatic groups to be introduced between iron centres have been chosen in order to keep the rigid-rod geometry of the carbon chain, to increase the chemical stability of the compounds and to maintain a high level of electronic coupling. The availability of compounds that differ for the aryl core in their bridge and the metal ancillary ligands allows discussion of the effects of structural and electronic molecular features on the extent of metal–metal communication. Particularly interesting are the effects on the metal–metal interaction resulting from (i) the replacement of a thiophenyl core by a phenyl core, a structural change in the bridge which does not greatly affect the intermetallic distance, (ii) the insertion of a 4,4'-biphenyl core, which significantly increases the length of the hydrocarbon linker and (iii) the presence of different ancillary ligands, that is CO and dppe.

The physical–chemical study was performed by electrochemical (CV) and spectroscopic techniques [IR, near infrared (NIR), UV/Vis] on selected synthesised dppe complexes.

Cyclic voltammetry (CV) results give information on the stability of the oxidation products but are not sufficient to determine the extent of electronic coupling between the metal termini. Actually, in a typical redox process involving symmetric bimetallic complexes, the separation between the two subsequent reversible waves, in the chemical and electrochemical sense, ΔE° , allows a quantitative estimate of the thermodynamic stability of the intermediate oxidation state with respect to disproportionation (i.e., the comproportionation constant K_c).^[10] ΔE° is only a qualitative indicator of an interaction between the two sites. According to the classification proposed by Robin and Day,^[10a] ΔE° values close to zero are characteristic of noninteracting metal sites, that is of class I complexes. Small ΔE° separations correspond to a weak interaction between the metals and this situation is described by a mixed-valence state involving trapped-valence systems (class II). Finally, larger ΔE° values correspond to a stabilisation of the mixed-valence complexes involving the totally delocalised class III systems. Although the larger the conjugation along the intermetallic bridge is, the easier the transfer of electronic information between metal centres is, the greater ΔE° tends to be, the more CV separations are influenced by other factors, in particular the medium (solvent and support electrolyte), which can modify the electrostatic interaction in the dications.^[10n] Thus, the CV analysis should always be integrated with spectroscopic investigation, in particular in the NIR region where mixed-valence species typically absorb.

While CV provides no information on the thermodynamic stability in the carbonylated species because of the irreversible nature of their waves, the dppe derivatives are studied in detail. In particular, the two dppe-substituted compounds, including the thiophenyl core and the 4,4'-biphenyl core respectively, exhibit very different reversible electrochemical behaviour. Thus they were also chemically

oxidised and their products were studied by near infrared (NIR) spectroscopy. A quenching of the NIR absorption band, which is characteristic of mixed-valence species, occurs when the thiophenyl core is replaced by the 4,4'-biphenyl moiety.

Theoretical calculations, based on state-of-the-art density functional theory (DFT) methods, were carried out on selected (PH₃)₂ and (CO)₂ model derivatives and provided (i) reliable structures for the title complexes, for which crystallographic data are not available yet, (ii) a detailed description of the electronic structure of the neutral and radical cation species, and (iii) prediction and interpretation of the experimental NIR bands based on the model radical cations.

Results and Discussion

The synthesis of dppe-substituted bimetallic compounds **7a–g** (Scheme 2) was first attempted using the EOP synthetic strategy outlined in path a₂ of Scheme 1; however, all the attempts to couple CpFe(dppe)I (**4**) with the different in situ generated Bu₃Sn–C≡C–Ar–C≡C–SnBu₃ (**3a–g**) in the presence of Pd failed (step 3 of path a₂). The failure in the formation of the Fe–C≡C bond was probably due to the strong electron-donating effect of dppe groups on the metal, which decreases the electrophilicity of the Fe–I bond, a basic requirement for oxidative addition to the Pd catalyst, thus the disclosure of the coupling process leading from **4** and **3a–g** to **7a–g**.^[7j,11]

As direct EOP formation of **7a–g** proved not to be possible, we decided first to form the (CO)-substituted bimetallic compounds **6a–g**, then to subject these compounds to photolytic substitution in the presence of dppe as reported for similar compounds.^[7d,12]

Synthesis of (CO)-Substituted Bimetallic Compounds **6a–g**

In Scheme 2 the EOP route to the bimetallic compounds **6a–g** and the subsequent conversion into the dppe derivatives **7a–g** are outlined. The EOP transformations were performed in dioxane solvent using 2–4% of Pd⁰ catalyst (single addition at the beginning of step 1). While step 1 and step 2 were rapidly accomplished (20–30 min overall time) with quantitative formation of **3a–g**, the accomplishment of step 3 was revealed to be a critical event because of the delicate nature of the bimetallic complexes **6a–g**. Although the reaction temperature was lowered to 50–80 °C, with consequent prolongation of reaction times, monitoring of the reaction progress by ¹H NMR revealed that formation of the expected product was always accompanied by unidentified side products and a small amount of starting materials always remained.

Isolation of products **6a–g** was not straightforward. Chromatographic separation proved to be always detrimental, therefore products had to be isolated and purified by repeated crystallisation (see Experimental Section), which affected the yields of recovered products.

Synthesis of (dppe)-Substituted Bimetallic Compounds **7a,d,g**

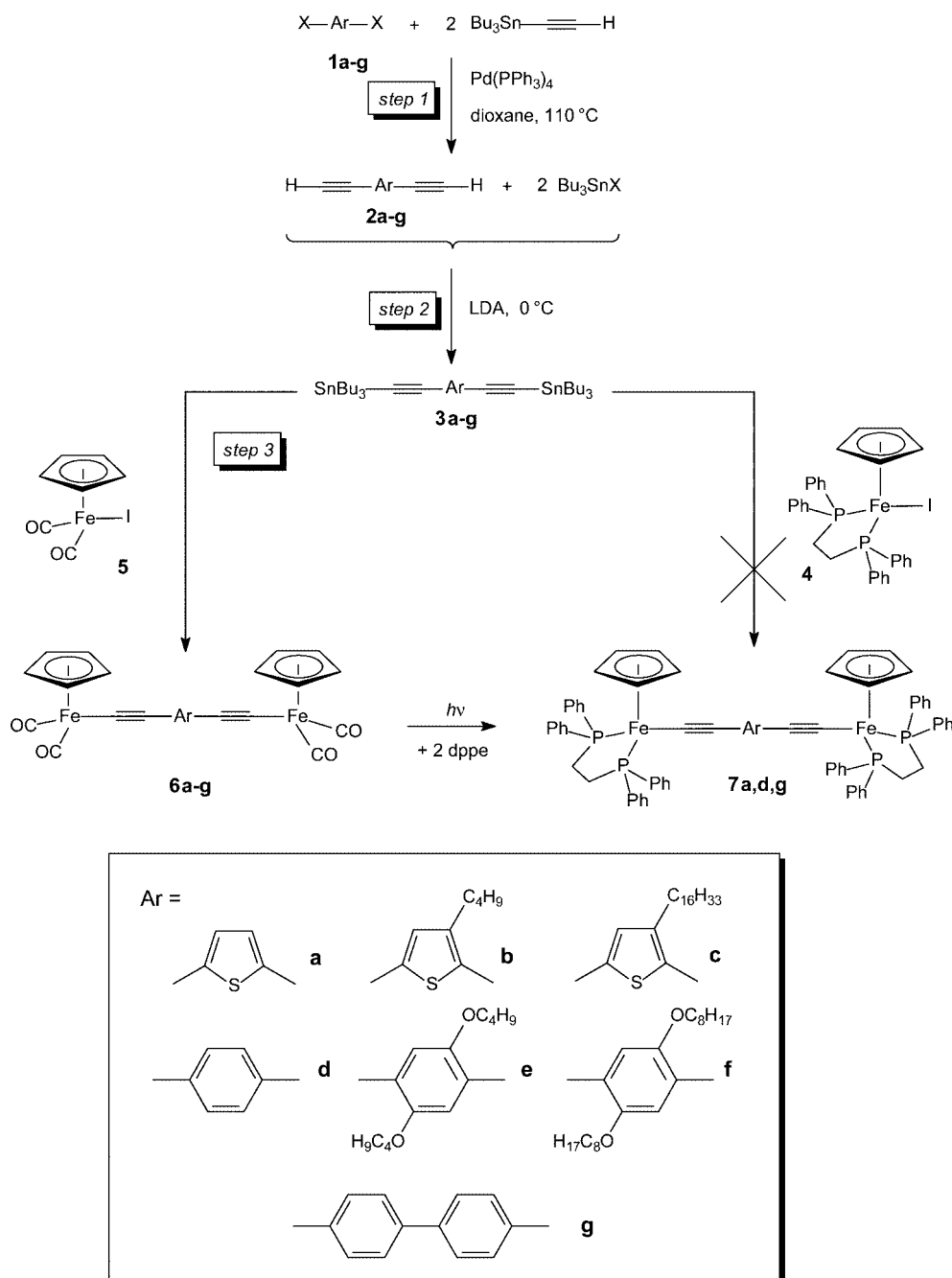
Complexes **6a,d,g** were subjected to ultraviolet irradiation (Scheme 2) to obtain the corresponding dppe-substituted bimetallic complexes. All reactions were carried out in distilled benzene using an equivalent amount per iron centre of 1,2-bis(diphenylphosphanyl)ethane, which readily replaces all the carbonyl groups.

Concerning the recovery of products in a pure form, chromatographic purification proved always too aggressive, and isolation of complexes **7a,d,g** was achieved only by repeated cycles of precipitation from hexane and following

dissolution of residues in toluene (or benzene), which allowed free dppe to be removed. By this method, products could be isolated and obtained in a satisfactory pure state, but the numerous cycles of precipitation/dissolution caused the yields to be drastically decreased.

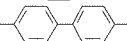
Cyclic Voltammetry (CV)

The CV at the platinum electrode, at scan rate 0.1 V s^{-1} , of a 2-mM solution of complex **7a** in CH_2Cl_2 in the presence of 0.1 M $n\text{Bu}_4\text{NPF}_6$ exhibits two reversible (in the chemical and electrochemical sense) one-electron waves at $E_{\text{pa}} =$



Scheme 2.

Table 1. Cyclic voltammetric data for $[\text{Cp}(\text{dppe})\text{Fe}-\text{C}\equiv\text{C}-\text{Ar}-\text{C}\equiv\text{C}-\text{Fe}(\text{dppe})\text{Cp}]^+[\text{BF}_4^-]$.^[a]

Complex	Ligand L_2	Spacer Ar	$\Delta E^0 = E_2^0 - E_1^0$ ^[b]	$E_1^0(0/+1)$ ^[b]	$E_{\text{pa}}-E_{\text{pc}}$ ^[c]	$E_2^0(+1/+2)$ ^[b]	$E_{\text{pa}}-E_{\text{pc}}$ ^[c]
7a	dppe		0.29	-0.19	56	0.10	70
7d	dppe		0.22	0.09	60	0.31	60
7g	dppe		–	0.04	70	–	–

[a] Solvent $\text{CH}_2\text{Cl}_2/0.2 \text{ M } n\text{Bu}_4\text{NBF}_4$; potential scan rate 0.1 V s^{-1} at a 0.5-mm diameter platinum disk electrode; $T = 20 \text{ }^\circ\text{C}$. [b] Volts vs. SCE. [c] Data are in mV.

-0.16 V and 0.14 V versus saturated calomel electrode (SCE), current ratio ($i_{\text{pa}}/i_{\text{pc}}$) = 1 (Figure 1, a). These two waves correspond to the formation of **7a**⁺ and **7a**²⁺. The anodic and cathodic peak separations ($E_{\text{pa}}-E_{\text{pc}}$) are 56 and 70 mV at scan rate 0.1 V s^{-1} (Table 1).

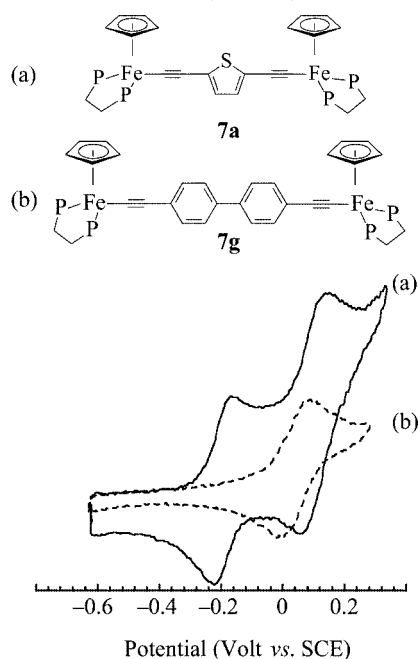


Figure 1. Cyclic voltammetric scan at a 0.5-mm diameter platinum disk electrode, $T = 20 \text{ }^\circ\text{C}$. Solvent $\text{CH}_2\text{Cl}_2/0.1 \text{ M } n\text{Bu}_4\text{NBF}_4$; scan rate of 0.1 V s^{-1} ; (a) solid line, $1 \text{ mM } \mathbf{7a}$; (b) dashed line, $1 \text{ mM } \mathbf{7g}$.

Similarly the CV of complex **7d** in the same conditions is characterised by two reversible one-electron waves in the oxidation scan from 1.5 to -1.5 V ($E_{\text{pa}} = 0.12 \text{ V}$ and 0.34 V vs. SCE) and shows a wave separation ΔE^0 of 0.22 V and peak separations ($E_{\text{pa}}-E_{\text{pc}}$) of 60 mV (Table 1). On the contrary, the CV of complex **7g** (Figure 1, b) reveals only one reversible wave at $E_{\text{pa}} = 0.08 \text{ V}$ with ($E_{\text{pa}}-E_{\text{pc}}$) = 70 mV and current ratio ($i_{\text{pa}}/i_{\text{pc}}$) = 1 (Table 1).

The low values of the oxidation potentials show that these binuclear complexes are electron-rich compounds. More interesting the quite large wave separations found for complexes **7a** and **7d** ($\Delta E^0 = 0.29 \text{ V}$ and 0.22 V , respectively) reveal a significant degree of metal–metal interaction when the 2,5-thiophene and 1,4-phenylene groups are present in the diethynylaryl spacer. The presence of a single wave in the CV of complex **7g** suggests that the intercal-

ation of a 4,4'-biphenyldiyl spacer drastically reduces the electronic communication between the metal sites.

We have also measured by CV the CO-substituted precursors **6a–g**. Such compounds are unstable in redox cycles, as expected from the absence of the bidentate phosphane ligands, which guarantee the reversibility of the process for **7a,d,g**. As a consequence, the possibility of obtaining analogous information about their electrical behaviour and the metal–metal electronic interaction is compromised. The CVs of all (CO)-substituted complexes (except for **6c**, this compound is very weakly soluble in most of the commonly used solvents) are characterised in the anodic scan by two irreversible waves. The CV in Figure 2 (a) is representative of the anodic scan of complexes **6a,b** and **6d–g**; in Table 2 the values of E_{p} are reported. The first waves correspond to the formation of $[\text{Cp}(\text{CO})_2\text{Fe}-\text{C}\equiv\text{C}-\text{Ar}-\text{C}\equiv\text{C}-\text{Fe}(\text{CO})_2\text{Cp}]^+$ in the range of $E_{\text{p}} = 0.84\text{--}1.15 \text{ V}$; potentials as high as expected on the basis of the electron-poor nature of the $\text{CpFe}(\text{CO})_2$ moiety. Concerning the second oxidation waves, they cannot be definitely assigned to the formation of $[\text{Cp}(\text{CO})_2\text{Fe}-\text{C}\equiv\text{C}-\text{Ar}-\text{C}\equiv\text{C}-\text{Fe}(\text{CO})_2\text{Cp}]^{2+}$ because of the irreversible nature of the preceding peaks. It is easily seen from Figure 2 that the height of the second oxidation peak is noticeably smaller than that of the first oxidation peak. The CVs at higher scan rates up to 100 V s^{-1} did not

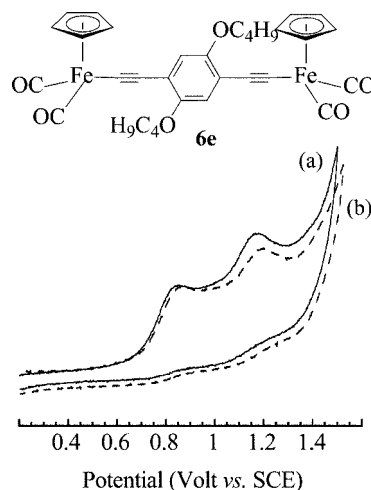
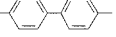


Figure 2. Cyclic voltammetric scan of $1 \text{ mM } \mathbf{6e}$ at a 0.5-mm diameter platinum disk electrode, $T = 20 \text{ }^\circ\text{C}$. Solvent $\text{CH}_2\text{Cl}_2/0.1 \text{ M } n\text{Bu}_4\text{NBF}_4$; (a) solid line, scan rate of 0.1 V s^{-1} ; (b) dashed line, scan rate 0.5 V s^{-1} .

allow unequivocal analysis of the variation of the intensity of the second waves because of the intrinsic slowness of the corresponding electron transfer. However, by increasing the scan rate from 0.1 to 0.5 V s⁻¹, the intensity of this wave, $i \times \nu^{-1/2}$ (ν = scan rate), decreases (Figure 2, b). One can suggest that the second oxidation process does not correspond to the oxidation of the radical cation of the neutral ethynylaryl binuclear complexes, but rather indicates the oxidation of other intermediates formed at the potential of the first wave. In this context, the separation between the two subsequent waves does not furnish sound information on the electronic interaction between the CpFe(CO)₂ units.

Table 2. Cyclic voltammetric data for [Cp(CO)₂Fe–C≡C–Ar–C≡C–Fe(CO)₂Cp]⁺[BF₄]⁻.^[a]

Complex	Ligand L ₂	Spacer Ar	R	E ₁ ⁰ (0/+1) ^[b]	E ₂ ⁰ (+1/+2) ^[b]
6a	(CO) ₂		/	0.84	1.33
6b	(CO) ₂		C ₄ H ₉	0.90	1.21
6d	(CO) ₂		/	0.89	1.31
6e	(CO) ₂		C ₄ H ₉	0.85	1.18
6f	(CO) ₂		C ₈ H ₁₇	0.87	1.14
6g	(CO) ₂		/	1.15	1.32

[a] Solvent CH₂Cl₂/0.2 M *n*Bu₄NBF₄; potential scan rate 0.1 V s⁻¹ at a 0.5-mm diameter platinum disk electrode; *T* = 20 °C. [b] Volts vs. SCE.

IR, UV/Vis, NIR Analysis

The mixed-valence radical cation **7a⁺** was generated at room temperature in CH₂Cl₂ by chemical oxidation of a 3.4-mm wine-coloured solution of the neutral complex with 1 equiv. of decamethylferrocenium tetrafluoroborate, [Fe(Cp*)₂][BF₄] {Cp* = C₅(CH₃)₅}. The resulting solution was deep-blue coloured.

The IR analysis of **7a⁺** shows a single vibration mode for the C≡C stretches (1981 cm⁻¹), at an intermediate frequency between those found for **7a** (2031 cm⁻¹) and **7a²⁺** (1929 cm⁻¹). Averaging of the vibration modes of the triple bonds is expected in homobimetallic class III complexes containing a polyalkynyl bridge, as the unpaired electron is fully delocalised and the resulting structure is symmetrical.

Conversely, for the previously reported [Cp*(dppe)Fe–C≡C–Ar–C≡C–Fe(dppe)Cp*] analogue (Ar = 2,5-C₄H₂S), Lapinte and co-workers^[7h] found that the two metal sites are not equivalent on the basis of the presence of two separate C≡C vibration modes in the IR spectrum (1983 and 1927 cm⁻¹), predicting that the unpaired electron is partially localised on the IR time scale (10⁻¹³ s). Alternatively, in this latter case, the lower energy band could not be a consequence of a symmetry breaking associated with the localisation of the odd electron. Possibly this band could be due to a Fermi coupling or to a harmonic combination with

another absorption mode at lower energy.^[13] These results reveal that substitution of the Cp* with the Cp groups in the metal sites renders more efficient the electronic coupling between the metal groups, the difference presumably coming from the metal/carbon ratio in the frontier orbitals because of the presence of the methyl groups.

The NIR spectrum of **7a⁺** (Figure 3) displays a band with a maximum at 5640 cm⁻¹ and a shoulder at 6500 cm⁻¹.

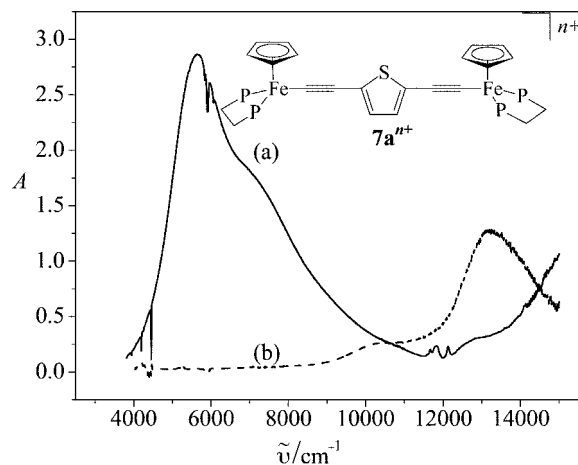


Figure 3. NIR spectra in CH₂Cl₂ at 20 °C of (a) 3.41 mM **7a⁺** and (b) **7a²⁺**; optical path, *b* = 0.100 cm.

The bands in this spectral region are considered diagnostic for an intervalence transfer process.^[10] A detailed theoretical overview on the presence of two or more bands, as previously discussed for the closely related Cp* derivatives^[7h] and other mixed-valence complexes,^[8a] is given by Meyer et al.^[11] As shown in Figure 4, the deconvolution of the spectrum has been satisfactorily obtained by considering three Gaussian components (5500, 6500, 7900 cm⁻¹) and the tail of the UV/Vis absorption. The effect of the polarity and ionic strength of the medium, which is generally employed to distinguish between class II and class III behaviour, was tested. The spectra of **7a⁺** in CH₃CN (ϵ = 37.5) and CH₂Cl₂ (ϵ = 10.7) are almost identical, that is no variation of the band energy and shape was observed. Moreover, there is no dependence of the band energy and shape on ionic strength up to an electrolyte concentration of 0.2 M in [*n*Bu₄N][BF₄].^[6i,7h,10] The analysis of the bands gives a bandwidth for the lower energy band I (Figure 4), $\Delta\tilde{\nu}_{1/2}$ = 1000 cm⁻¹, which is much below the theoretical value (3630 cm⁻¹) predicted by the Hush equation for a localised mixed-valence (class II) symmetric system,^[14] $\Delta\tilde{\nu}_{1/2}$ = (2310 $\tilde{\nu}_c$)^{1/2} cm⁻¹, where $\tilde{\nu}_c$ is the frequency of the maximum. By analogy with the data reported by Lapinte and co-workers on the Cp* analogues,^[7h] band I of **7a⁺** could be an intervalence transfer (IT) transition and **7a⁺** is assigned to class III, at least on the timescale of the NIR spectroscopy (10⁻¹⁴ s). The value of the *H*_{ab} parameter,^[14,15] calculated using the formula H_{ab} (cm⁻¹) = $\tilde{\nu}_{max}/2$, is 2750 cm⁻¹.

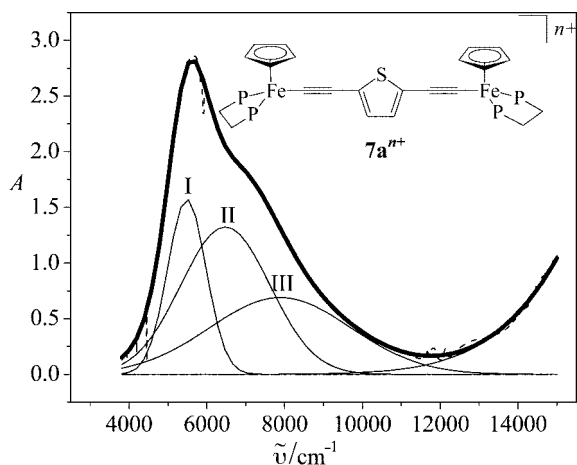


Figure 4. Gaussian deconvolution of the NIR bands of $7a^+$ (dashed line, experimental curve; solid lines, deconvoluted bands I, II, III; bold line, the sum of I, II, III components).

The addition either in CH_3CN or CH_2Cl_2 of a second equivalent of ferrocenium, whose oxidation potential is sufficiently high to oxidise the second metal group forming a green solution of $7a^{2+}$, causes the disappearance of the bands of the monocation and the appearance of a less intense absorption at 13100 cm^{-1} (Figure 3), likely because of a ligand-to-metal charge transfer (LMCT) transition. Under the same condition, we have found that Cp_2Fe^+ and $Cp^*_2Fe^+$ show bands at 13600 and 12900 cm^{-1} respectively.

Also the oxidation of $7g$ was monitored by NIR spectroscopy (Figure 5). The oxidation with 1 equiv. of ferrocenium gives a green solution whose spectrum in this region presents a very weak band at about 6000 cm^{-1} and a more intense band at 12500 cm^{-1} , which could be assigned to the IT process of $7g^+$ and to an LMCT transition of the dication $7g^{2+}$, respectively, indicating that the mixed-valence state is not stable with respect to the disproportionation to the $7g$ and $7g^{2+}$ states, in agreement with the presence of a single oxidation wave in the CV of complex $7g$.

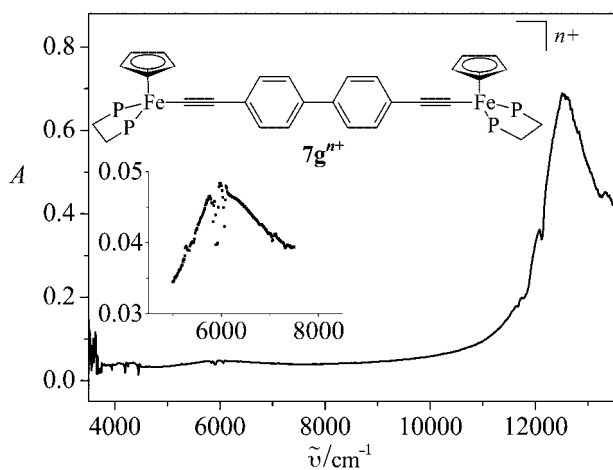


Figure 5. NIR spectra in CH_2Cl_2 at $20\text{ }^\circ\text{C}$ of 3.4 mM $7g$ oxidised with 1 equiv. of ferrocenium.

The couple $7a/7a^+$ was also studied in the UV/Vis spectroscopic region. The solution of $7a$ in CH_2Cl_2 presents a very strong absorption at $\lambda = 410\text{ nm}$, a wavelength quite similar to that reported for the Cp^* analogue (418 nm), and attributed to a metal-to-ligand charge transfer (MLCT) transition.^[7b] The spectrum of the deep-blue solution of $7a^+$ is totally different from its precursor $7a$. In fact, two new strong bands appears at 612 and 765 nm, which are responsible for the deep-blue colour of the mixed-valence species. They might be ascribed to LMCT transitions, similarly to what Lapinte and co-workers previously proposed for the absorptions at 588 and 653 nm of the Cp^* mixed-valence analogous species.^[7b] In that case, the intense MLCT transition observed for the neutral complex is still present in the spectrum of the monocation at a slightly red-shifted wavelength (423 nm), indicating that the characteristic absorptions of both Fe^{II} and Fe^{III} metal groups coexist (trapped valence, class II). On the contrary, in the UV/Vis spectrum of $7a^+$ the MLCT band, which is characteristic of a Fe^{II} species, is absent, clearly showing that in $7a^+$ the valence is delocalised on the very fast UV/Vis timescale (10^{-15} s).

Density Functional Theory (DFT) Analysis

In order to gain insight on the factors ruling the extent of electronic communication and possibly to deconvolute the effects due to the structural parameters (i.e., metal-metal distance) from those related to the peculiar electronic features (i.e., the nature of the bridge and the nature of the ancillary ligands), we investigated systematically selected model complexes by DFT calculations.^[16]

DFT optimisations were performed at B3LYP/LANL2DZ,6-31G** level of theory without any restriction in symmetry and tight conditions (see Computational Details) for neutral and oxidised PH_3 analogues of $7a^{0/+1}$, $7d^{0/+1}$ and $7g^{0/+1}$, which differ in the nature of the conjugated spacer. A *transoid* conformation of the metal centres is found to be more stable for PH_3-7a and PH_3-7d . Instead, in the fully optimised PH_3-7g the phenyl rings are oriented in distorted *cisoid* conformation.^[17] It is worth noticing that the orientation of the metal fragments is such that the plane of the aromatic cores bisects the dihedral angle P-Fe-P. Consequently the conformation calculated for PH_3-7g is directly related to the torsion angle between the two phenyl rings. The calculated geometries of the neutral complexes are shown in Figure 6 (I-III). Significant interatomic distances and bond angles are reported in Table 3. In several cases the crystallographic data of structurally similar compounds are indicated and the good agreement with the analogous computed parameters enhances our confidence in the quality of the optimised geometries. A distinct alternation of single and multiple bonds is predicted in the three complexes. The average bond length of the alkyne units of the linkers is 1.232 \AA , a value that nicely compares to the triple bond length in acetylene, that is 1.212 \AA . The localised double bonds of the rings have an average value of 1.386 \AA , which is also comparable to the ethylene double bond length (1.320 \AA).

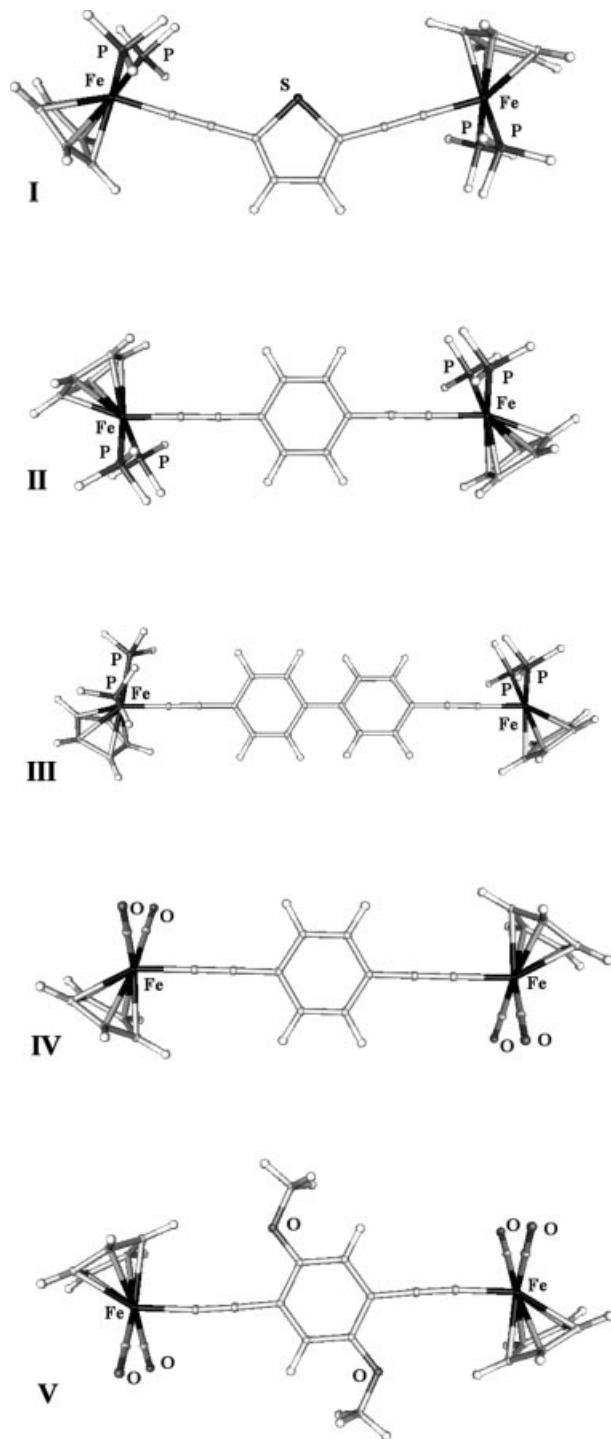


Figure 6. Calculated molecular structures of neutral model complexes: $\text{PH}_3\text{-7a}$ (I), $\text{PH}_3\text{-7d}$ (II), $\text{PH}_3\text{-7g}$ (III), **6d** (IV) and $\text{CH}_3\text{O-6e}$ (V). Heteroatoms are labelled for sake of clarity.

The ground-state electronic structures of $\text{PH}_3\text{-7a}$, $\text{PH}_3\text{-7d}$ (the electronic structure of this complex was previously reported by Lapinte et al.^{[70])} and $\text{PH}_3\text{-7g}$ exhibit similar features.

Several authors have reported their theoretical studies on polyalkynyl- and alkynylaryl-bridged bimetallic complexes; thus the bonding between group 8 metal centres and ace-

tylides is well documented.^[18] A qualitative fragment analysis reveals that the cationic $[\text{Cp}(\text{PH}_3)_2\text{Fe}]^+$ fragments bond by strong σ -type interactions between unoccupied high-lying metallic frontier orbitals and low-lying occupied orbitals of the bridge (electron donation from the bridge to the metal fragments). Metal-carbon π -type interactions occur between occupied metal frontier orbitals and unoccupied carbon levels (weak π -type back-donation). The Kohn-Sham HOMOs are mainly localised on the metal centres and the ethynyl groups, and, to a less extent, on the aromatic rings. They result from out-of-phase combination of metal $d\pi$ orbitals and out-of-plane π orbitals of the linker; they exhibit *anti* bonding character between adjacent multiple bonds. The LUMO and LUMO+1 are almost degenerate and localised on the metal fragments. The topologies of Kohn-Sham frontier orbitals of $\text{PH}_3\text{-7d}$ are shown in Figure 7.

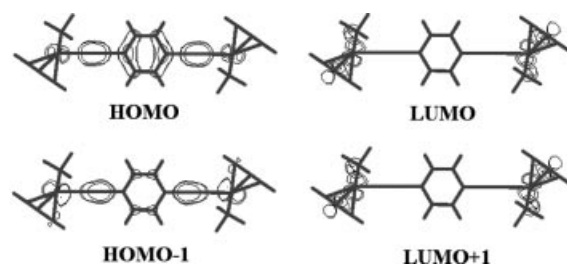


Figure 7. Top view of the contour plot of the frontier Kohn-Sham MOs of $\text{PH}_3\text{-7d}$. Contour values are ± 0.035 , ± 0.04 and ± 0.05 ($e/\text{bohr}^3)^{1/2}$.

A rather large energy gap separates the occupied and empty orbital sets in $\text{PH}_3\text{-7a}$, $\text{PH}_3\text{-7d}$ and $\text{PH}_3\text{-7g}$ (see Figure 8). The HOMO-LUMO gap in $\text{PH}_3\text{-7d}$ is larger by about 0.2 eV than that of $\text{PH}_3\text{-7a}$ (3.50 vs. 3.30 eV), and this is mainly due to the fact that the energy of HOMO of $\text{PH}_3\text{-7d}$ is lower than that of HOMO of $\text{PH}_3\text{-7a}$. The HOMO-LUMO gap of $\text{PH}_3\text{-7g}$ is 3.69 eV.

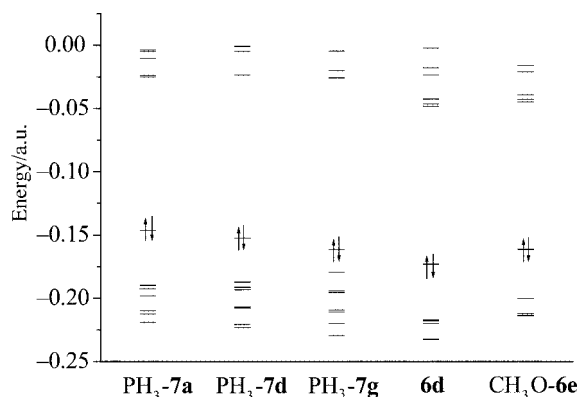
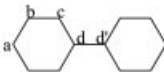


Figure 8. Frontier MOs for complexes $\text{PH}_3\text{-7a}$, $\text{PH}_3\text{-7d}$, $\text{PH}_3\text{-7g}$, **6d** and $\text{CH}_3\text{O-6e}$. HOMOs are indicated by double occupancy arrows; bold lines indicate almost degenerate energy levels.

Upon oxidation no significant conformational changes are observed. Both in $\text{PH}_3\text{-7a}^+$ and $\text{PH}_3\text{-7d}^+$ the metal units

Table 3. Selected interatomic distances [Å] and angles [°] for the neutral and oxidised complexes PH₃-7a^{0/+1}, PH₃-7d^{0/+1} and PH₃-7g^{0/+1}.

	PH ₃ -7a ^{0/+1}		PH ₃ -7d ^{0/+1}		PH ₃ -7g ^{0/+1}	
Fe1–Fe2	11.315	Fe1–Fe2	12.008	Fe1–Fe2	16.342	
	11.234		11.853		16.197	
Fe–P ^[a]	2.206	Fe–P ^[a]	2.200 (2.187 ^[b])	Fe–P ^[a]	2.203	
	2.221		2.221		2.219	
Fe–C _α ^[a]	1.915	Fe–C _α	1.918	Fe–C _α	1.917	
	1.856		1.860		1.868	
Fe–Q ^[a]	1.771	Fe–Q ^[a]	1.768 (1.738 ^[b])	Fe–Q ^[a]	1.769	
	1.773		1.772		1.773	
C _β –C ^[a,c]	1.408	C _β –C ^[a,c]	1.426 (1.42 ^[d])	C _β –C ^[a,c]	1.426	
	1.378		1.399		1.405	
C _α ≡C _β ^[a,e]	1.233	C _α ≡C _β ^[a,e]	1.232 (1.23 ^[d])	C _α ≡C _β ^[a,e]	1.231	
	1.247		1.244		1.242	
						
S–C _a	1.765	C _a –C _b	1.412	C _a –C _b	1.411	
	1.766		1.426		1.421	
C _a –C _b	1.384	C _b –C _c	1.388	C _b –C _c	1.389	
	1.386		1.376		1.380	
C _b –C _c	1.416	C _c –C _d	1.412	C _c –C _d	1.407	
	1.413		1.426		1.418	
				C _d –C _{d'}	1.481	
					1.461	
				θ ^[f]	34.5	
					24.2	
γ ^[g]	178.2	γ ^[g]	180.0	γ ^[g]	33.8	
	170.8		180.0		24.5	

[a] Average values. [b] X-ray data of (η⁵-C₅Me₅)(η²-dppe)Fe–C≡C–C₆H₅.^[7j] [c] Single C_β–C bond in the ethynyl bridge. [d] Average crystallographic values of [Fe(η⁵-C₅Me₅)(η²-dppe)(C≡C)]₃(μ-1,3,5-C₆H₃).^[7o] [e] Triple C_α≡C_β bond in the ethynyl bridge. [f] Torsion angle between the two rings, around the bond C_d–C_{d'}. [g] By indicating the centroids of the Cp rings as Q and Q', a torsion angle γ can be defined as Q–Fe1–Fe2–Q', so that γ = 0 corresponds to a *cis* conformation of the metal termini and γ = 180 indicates a *trans* conformation.

are still oriented *trans* with respect to the bridging ligand, while in PH₃-7g⁺ the *cisoid* conformation is still more stable. Upon going from the neutral to the corresponding oxidised species, the Fe–C_α bond and the bond between C_β and the adjacent carbon atom of the aryl core shorten, while the alkyne bond C_α≡C_β elongates. The cation PH₃-7a⁺ is generated by removal of one electron from the HOMO of the neutral parent compound. In PH₃-7d⁺ and PH₃-7g⁺ there is a rearrangement of the energy levels, because their HOMOs (118β and 138β) correspond to HOMOs–1 of the neutral parent complexes. The trend in stability, based on the HOMO–LUMO gap, is inverted in the series of cations, PH₃-7a⁺ being the most stable, as expected on the basis of the lower resonance energy of the thiophenyl unit compared to that of the phenyl unit, because of the mixing of sulfur d orbitals with carbon π

orbitals. The HOMOs of the cations PH₃-7d⁺ and PH₃-7g⁺ are characterised by an in-phase contribution of metal dπ orbitals disposed in an *anti* bonding fashion with respect to the out-of-plane π orbitals of the linker. While the extent of delocalisation is large in PH₃-7a⁺, the contribution of p(π) carbon orbitals of the phenyls to HOMO is poorer both in PH₃-7d⁺ and PH₃-7g⁺. The Kohn–Sham HOMOs of PH₃-7a⁺, PH₃-7d⁺ and PH₃-7g⁺ are shown in Figure 9.

The effect of replacing the ancillary ligands PH₃ with CO groups was investigated theoretically on the couple 6d^{0/+1} by direct comparison with PH₃-7d^{0/+1}. In addition, the influence of alkoxy groups on the phenyl core was explored by calculating the electronic structures of the methoxy analogues of 6e^{0/+1}, to be compared with those of 6d^{0/+1}. The full geometry optimisations of 6d^{0/+1} and of CH₃O-6e^{0/+1} were calculated at B3LYP/LANL2DZ,6-31G** level of

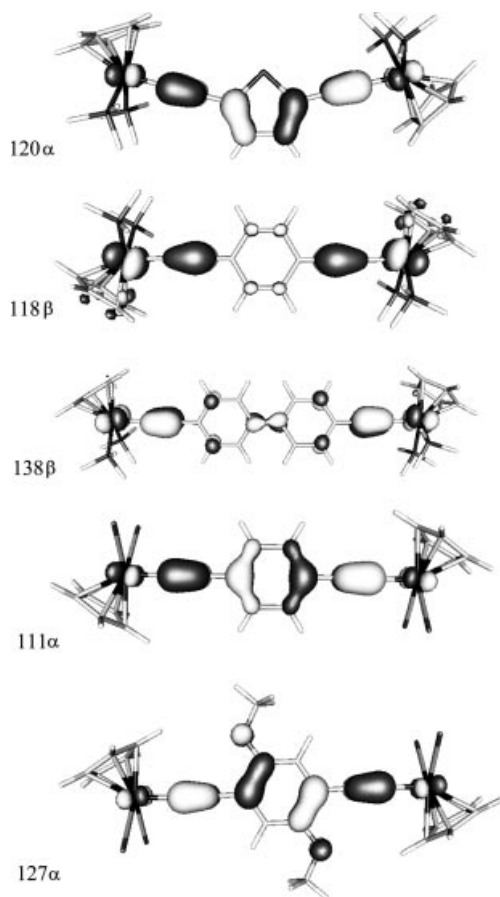
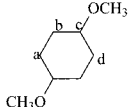


Figure 9. Kohn-Sham HOMOs of $\text{PH}_3\text{-7a}^+$, $\text{PH}_3\text{-7d}^+$, $\text{PH}_3\text{-7g}^+$, $\mathbf{6d}^+$ and $\text{CH}_3\text{O-6e}^+$. Surface values are $0.04 \text{ (e/bohr}^3)^{1/2}$.

theory. The neutral species are shown in Figure 6 (IV, V) and their significant structural data are reported in Table 4. The full optimisations converged in both neutral complexes with a *trans* conformation of the metal groups. As for the PH_3 neutral derivatives, the calculations predict a distinct alternation of adjacent single and multiple bonds (see Table 4). In particular, a contraction of the alkyne bond length $\text{C}_\alpha\equiv\text{C}_\beta$ is observed compared to the PH_3 -substituted species, which is a consequence of the electron density loss of the metal (1.225 vs. 1.232 Å).

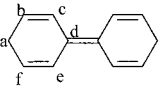
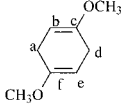
Another effect of replacing the phosphanes with carbonyl groups is a reduction in energy of the frontier orbitals, as expected on the basis of the electron-poorer nature of the metal centres in the carbonylated complexes due to backbonding from the occupied metal orbitals to the empty π^* of the carbonyl ligands (Figure 8). The HOMOs of $\mathbf{6d}$ and $\text{CH}_3\text{O-6e}$, resulting from out-of-phase combination of metal $d\pi$ orbitals and out-of-plane π orbitals of the linker, are strongly localised on the bridge, with minor metal contribution, and show *anti* bonding character between adjacent multiple bonds. The LUMOs and LUMOs+1 are almost degenerate and localised on the end-capping termini. The HOMO–LUMO gap of $\text{CH}_3\text{O-6e}$ (3.17 eV) is smaller than that of $\mathbf{6d}$ (3.39 eV) and this is mainly the result of the destabilisation of the HOMO of the former complex, caused by the presence of the methoxy substituents (Figure 8). The variation in bond lengths occurring upon oxidation is reported in Table 4. No rearrangements of the frontier electronic levels are observed: the electron is removed from the HOMO of the neutral parent compound, as found for $\text{PH}_3\text{-7a}$.

Table 4. Selected interatomic distances [Å] and angles [°] for the neutral and oxidised complexes $\mathbf{6d}^{0/+1}$ and $\text{CH}_3\text{O-6e}^{0/+1}$.

	$\mathbf{6d}$	$\mathbf{6d}^+$		$\text{CH}_3\text{O-6e}$	$\text{CH}_3\text{O-6e}^+$
Fe1–Fe2	11.970	11.851	Fe1–Fe2	11.930	11.858
Fe–C _{CO} ^[a]	1.770	1.786	Fe–C _{CO} ^[b]	1.768	1.783
Fe–C _α ^[a]	1.911	1.873	Fe–C _α ^[a]	1.906	1.878
Fe–Q ^[a]	1.778	1.775	Fe–Q ^[b]	1.778	1.774
C _β –C ^[a,b]	1.426	1.395	C _β –C ^[a,b]	1.422	1.394
C _α ≡C _β ^[a,c]	1.225	1.240	C _α ≡C _β ^[a,c]	1.224	1.236
					
C _a –C _b	1.411	1.429	O–C _c ^[a]	1.372	1.344
C _b –C _c	1.388	1.373	C _a –C _b	1.416	1.448
C _c –C _d	1.411	1.429	C _b –C _c	1.392	1.384
			C _c –C _d	1.409	1.414
γ ^[d]	121.9	174.8	γ ^[d]	174.9	179.5

[a] Average values. [b] Single C_β–C bond in the ethynyl bridge. [c] Triple C_α≡C_β bond in the ethynyl bridge. [d] By indicating the centroids of the Cp rings as Q and Q', a torsion angle γ can be defined as Q–Fe1–Fe2–Q', so that $\gamma = 0$ corresponds to a *cis* conformation of the metal termini and $\gamma = 180$ indicates a *trans* conformation.

Table 5. Mulliken spin densities.

	PH ₃ -7a ⁺	PH ₃ -7d ⁺	6d ⁺	PH ₃ -7g ⁺	CH ₃ O-6e ⁺
Fe1	0.197	0.244	0.102	0.219	0.065
Fe2	0.192	0.244	0.102	0.218	0.065
C _{α1} ^[a]	0.144	0.106	0.212	0.079	0.211
C _{β1} ^[b]	0.027	0.073	0.033	0.076	-0.001
C _{α2} ^[a]	0.143	0.106	0.212	0.079	0.211
C _{β2} ^[b]	0.030	0.073	0.033	0.076	-0.001
S	-	-	-	-	-
p ^[c]	0.046	-0.002	-	-0.002	-
C _{CO}	-0.0008	-	-0.005	-	-0.004
O _{CO}	-	-	-0.006	-	-0.005
O _{CH₃O}	-	-	-	-	0.045
					
C _a ^[c]	0.124	0.073	0.129	0.045	0.167
C _b ^[c]	0.053	0.016	0.021	0.022	0.096
C _c ^[c]	0.057	0.018	0.018	0.006	-0.076
C _d ^[c]	0.126	0.073	0.129	0.057	0.167
C _e ^[c]	-	0.016	0.021	0.005	0.096
C _f ^[c]	-	0.018	0.018	0.022	-0.076

[a] Alkyne carbon atom linked to iron. [b] Alkyne carbon atom linked to the aromatic ring. [c] Carbon atom of the aromatic core; the labelling is reported in the schemes above.

The extent of delocalisation of the unpaired electron in the radical cations was estimated on the basis of Mulliken spin densities, which are reported in Table 5.

The distribution of the spin density is symmetric in all the radical cations, although symmetry was not taken into account in the calculations. The spin density is well delocalised on the iron centres and on the C_α atoms in PH₃-7a⁺ and in PH₃-7d⁺. In PH₃-7a⁺ the spin density is distributed also on the carbon atoms adjacent to S in the thiophenyl core, while in both PH₃-7d⁺ and PH₃-7g⁺ the spin density values on the phenyl rings are rather small. In 6d⁺ and CH₃O-6e⁺ the significant decrease of the spin density on the metals as compared to PH₃-7d⁺ is accompanied by its increase on the two α carbons and on two carbon atoms of the rings (see Table 5).

The extent of delocalisation is in favour of a stronger metal–metal interaction,^[7m] and decreases in the PH₃ derivatives in the order PH₃-7a⁺ > PH₃-7d⁺ > PH₃-7g⁺, in agreement with the trend based on the experiments.

To investigate the presence and the nature of the NIR absorptions of these model di-iron cations we have carried out time-dependent density functional theory (TDDFT) calculations,^[19] which have been recently employed with success for mixed-valence organometallic species.^[20] The level of theory is B3LYP/LANL2DZ,6-31+G* (see Compu-

tational Details). The lowest excitation energy computed for PH₃-7a⁺ in the NIR region is 8560 cm⁻¹ (0.47), with an error comparable to those reported in a similar analysis.^[20a] It corresponds to the lowest energy deconvoluted experimental absorption at 5500 cm⁻¹. The detailed composition is shown in Table 6. Its most relevant components involve the couples of levels 120α–121α and 119β–120β, that is the highest occupied α/β levels and the lowest unoccupied α/β levels respectively (pictures of the couples of MOs involved in the calculated excitation energies are given in the Supporting Information), which have significant contributions from d orbitals of both iron centres and p(π) carbon orbitals of the bridge.

In the case of PH₃-7d⁺, an absorption is computed at 6859 cm⁻¹ (f = 0.62) corresponding mainly to the HOMO (118β)–LUMO (119β) transition. The experimental spectrum of the Cp* analogue of 7d⁺ exhibits a single band at 4960 cm⁻¹.^[7] Also in this case the couple of orbitals involved in the mono-electronic transition are delocalised all over the molecular backbone.

By TDDFT calculations we also found an allowed low-energy absorption for PH₃-7g⁺ at 5216 cm⁻¹ (f = 0.83) assigned mainly to HOMO (138β)–LUMO (139β) and HOMO–1 (137β)–LUMO (139β) transitions. This excitation energy in the NIR region corresponds to the weak

Table 6. NIR vertical excitation energies.

	PH ₃ -7a ⁺	PH ₃ -7d ⁺	PH ₃ -7g ⁺	6d ⁺	CH ₃ O-6e ⁺
HOMO–LUMO gap	1.525 eV ^[a]	1.452 eV ^[b]	0.886 eV ^[c]	1.474 eV ^[d]	1.451 eV ^[e]
Excitation energy					
[nm]	1168	1458	1917	871	809
[cm ⁻¹]	(8562)	(6859)	(5216)	(11481)	(12361)
Oscillator strength	0.47	0.62	0.83	0.52	0.39
Composition ^[f]	120α → 121α (0.296)	119α → 122α (0.258)	139α → 140α (0.239)	111α → 112α (0.277)	126α → 128α (0.101)
	108β → 120β (-0.104)	107β → 119β (-0.107)	132β → 139β (0.200)	111α → 116α (0.133)	127α → 128α (-0.300)
	116β → 123β (-0.161)	111β → 119β (-0.160)	135β → 140β (-0.149)	108β → 111β (-0.174)	126β → 127β (0.935)
	119β → 120β (1.006)	115β → 122β (-0.171)	138β → 139β (0.865)	110β → 111β (0.904)	
		118β → 119β (0.996)			

[a] The HOMO is 120α, the LUMO is 120β. [b] The HOMO is 118β, the LUMO is 119β. [c] The HOMO is 138β, the LUMO is 139β. [d] The HOMO is 111α, the LUMO is 111β. [e] The HOMO is 127α, the LUMO is 127β. [f] The most relevant mono-electronic transitions are indicated; values in brackets are the CI coefficients.

absorption experimentally detected for 7g⁺ around 6000 cm⁻¹. It should be noted that in PH₃-7d⁺ and PH₃-7g⁺ the strongest NIR absorptions have an important contribution from the HOMO–LUMO transition and are thus shifted toward lower frequencies, as compared to that of PH₃-7a⁺. Most importantly, no charge transfer character between the metal termini is observed, as reported recently for other organometallic binuclear systems,^[20a] but these NIR absorptions are better interpreted as allowed electronic transitions between filled and empty delocalised frontier levels. The oscillator strengths increase with the length of the alkynylaryl bridge, as already noticed in previous theoretical studies.^[20c,20d]

TDDFT calculations on the carbonylated model cations 6d⁺ and CH₃O-6e⁺ do not reveal any low-energy transition. In the former an absorption is predicted at 11481 cm⁻¹ (*f* = 0.52), while in the latter the calculated excitation energy is 12361 cm⁻¹ (*f* = 0.39). In both cases the transitions involve the highest occupied α/β levels and the lowest unoccupied α/β levels, as for PH₃-6a⁺. Also in these species no metal–metal charge transfer character is observed.

Conclusions

The combination of the EOP synthetic protocol and the Pd-catalysed metal–carbon bond formation procedure offers suitable synthetic access to a large family of bimetallic complexes (6a–g) characterised by the presence of different conjugated (bis-ethynyl)aromatic spacers bridging two iron centres. Our EOP synthetic route represents a complementary approach to alkynylaryl-bridged bimetallic complexes with respect to Lapinte's method.^[7q] In our procedure the straightforward formation of the bis(tributylethynyltin)aromatic derivatives 3a–g and their direct in situ use to form complexes 6a–g prevent the formation and isolation of the corresponding bis(trimethylsilylethynyl) derivatives as required by Lapinte's procedure.^[7u]

Although substitution of carbonyls with dppe is conveniently performed only in some cases, the dppe derivatives

of such organometallic assembly (7a,d,g) proved to be a useful manifold to study the electrical and optical properties of the conjugated spacer and the interaction between the metal centres, and thus, in perspective, the properties of polymeric materials incorporating such building blocks in the backbone.

On the basis of the electrochemical and optical properties of complexes 7a,d,g, a correlation between the extent of the metal–metal electronic interaction and the nature of the diethynylaryl bridge can be pointed out. In fact, the Δ*E*^o separations between the two subsequent reversible waves increase in the order 7a > 7d > 7g, as does the efficiency of the metal–metal electronic coupling. The previously reported [Cp*(dppe)Fe–C≡C–Ar–C≡C–Fe(dppe)–Cp*] analogue (Ar = 2,5-C₄H₂S) displayed a somewhat more pronounced Δ*E*^o (0.35 V) than 7a. This indicates a higher thermodynamic stability of the corresponding monocationic intermediate with respect to disproportionation, probably due to the electron-donating effect of the methyl substituents of Cp*, which stabilise the positive charge on the metal groups. A similar trend can be established on the basis of the spectroscopic results for the mixed-valence species 7a⁺, 7d⁺ and 7g⁺. In the case of 7a⁺, the IR data, the shape and the solvent effect of the NIR band and the UV/Vis spectrum indicate unambiguously that the cation is a delocalised (class III) mixed-valence system on the timescale of 10⁻¹⁵ s. The comparison with the analogous 2,5-bis{[η⁵-C₅(CH₃)₅]Fe(η²-dppe)(σ¹-C≡C)}-C₄H₂S, which is valence-trapped on the IR timescale, highlights the important effect of replacing Cp* with Cp in the metal termini. On the basis of its electrochemical behaviour and the spectroscopic data reported in the literature, 7d⁺ can also be assigned to class III. The analysis of 7g⁺ is less clear-cut, because of the low stability of this mixed-valence cation in solution. PH₃-7g⁺ has a certain extent of delocalisation, but the metal–metal interaction is hampered with respect to PH₃-7d⁺ because of the increase of the distance and the greater flexibility of the bridge. DFT calculations support the experimental findings and allow deconvolution

of geometric effects, such as the intermetallic distance ($\text{PH}_3\text{-7d}^+$ vs. $\text{PH}_3\text{-7g}^+$), from electronic effects, that is the different nature of the incorporated aryl core ($\text{PH}_3\text{-7a}^+$ vs. $\text{PH}_3\text{-7d}^+$), on the extent of electronic delocalisation. On the basis of the computational results on the carbonylated model cation $\mathbf{6d}^+$ a less efficient electron delocalisation is observed with respect to the corresponding PH_3 analogue ($\mathbf{6d}^+$ vs. $\mathbf{7d}^+$). In addition, in the presence of the methoxy substituents on the aryl core in $\text{CH}_3\text{O-6e}^+$ the spin density decreases further on the iron centres and moves to the phenyl ring ($\text{CH}_3\text{O-6e}^+$ vs. $\mathbf{6d}^+$).

TDDFT calculations predict that NIR absorptions, which are a sort of fingerprint of mixed-valence species, occur only in $\text{PH}_3\text{-7a}^+$, $\text{PH}_3\text{-7d}^+$ and $\text{PH}_3\text{-7g}^+$, and that they do not exhibit dominant charge transfer character between the metal termini, but are better described as allowed electronic transitions between filled and empty frontier levels.

Finally the efficiency of the dialkynyl–thiophenyl unit in conveying electron information is further recognised and associated to the large extent of delocalisation in the radical cations bearing this aryl core.^[61,6m] Work is in progress to employ this functional unit, intercalated also by different metal centres, in larger molecular wires.

Experimental Section

General: All manipulations were carried out under argon using Schlenk techniques. Dioxane and benzene were dried and distilled respectively over Na and Na/K alloy, and argon-saturated prior to use. The following chemicals were prepared according to the published procedure: 1,4-diiodo-2,5-dioctyloxybenzene,^[4] 1,4-diiodo-2,5-dibutoxybenzene,^[4] 2,5-diiodo-3-hexadecylthiophene^[4] and 2,5-diiodo-3-butylthiophene.^[4] Other chemicals were used as received. Routine NMR spectra were recorded with a AC-300 P Bruker spectrometer (300, 121 and 75 MHz respectively for ^1H , ^{31}P , ^{13}C). Chemical shifts are given in parts per million (ppm) relative to tetramethylsilane (TMS) for ^1H NMR and ^{13}C NMR spectra and 85% H_3PO_4 for ^{31}P NMR spectroscopy. Cyclic voltammograms [except the ones of complexes $\mathbf{6d,g}$ and $\mathbf{7a,d}$, performed by Dr. Mikhail G. Peterleitner of Nesmeyanov Institute of Organoelement Compounds (INEOS), Russian Academy of Science, Moscow] were recorded with an AMEL 500 potentiostat. Transmittance FTIR spectra were recorded with a Nicolet FT 510 instrument in the solvent subtraction mode, using a 0.1-mm CaF_2 cell. NIR spectra were recorded with a Bruker Equinox55 FTIR spectrometer equipped with an optical fibre for NIR measurements on liquids. Elemental analyses were performed by the Servizio Microanalisi of the Dipartimento di Chimica of Università di Roma “La Sapienza”.

2,5-Bis[($\eta^5\text{-C}_5\text{H}_5$) $\text{Fe}(\text{CO})_2(\sigma^1\text{-C}\equiv\text{C})$] $\text{C}_4\text{H}_2\text{S}$ (6a**). Step 1:** In a Schlenk tube $\text{Bu}_3\text{SnC}\equiv\text{CH}$ (0.962 g, 3.05 mmol), 2,5-diiodothiophene (0.500 g, 1.49 mmol) and $\text{Pd}(\text{PPh}_3)_4$ (40 mg, 0.035 mmol) were stirred in dioxane (30 mL) at 110 °C for 20 min.

Step 2: The brown solution was then cooled (ca. 0 °C) and LDA (1.8 mL, 2 M) was slowly added.

Step 3: This mixture was left for about 30 min at room temperature, ($\eta^5\text{-C}_5\text{H}_5$) $\text{Fe}(\text{CO})_2\text{I}$ (0.914 g, 3.01 mmol) was added and the resulting dark solution was heated (50 °C) for 7 h, then filtered through a thin Celite layer and dried under vacuum. The residue

was dissolved in a small amount of CH_2Cl_2 and then precipitated with pentane. After filtration and repeated washings with pentane, a dark brown powder (0.533 g, 74% yield) was obtained. IR (CH_2Cl_2): 2095 (w) $\tilde{\nu}_{\text{C}=\text{C}}$, 2044 (s), 2000 (s) $\tilde{\nu}_{\text{CO}}$ cm^{-1} . ^1H NMR (CDCl_3): δ = 6.60 (2 H, thioph.), 5.02 (10 H, Cp) ppm. Spectroscopic data correspond to the reported data.^[4]

2,5-Bis[($\eta^5\text{-C}_5\text{H}_5$) $\text{Fe}(\text{CO})_2(\sigma^1\text{-C}\equiv\text{C})$]-3-(C_4H_9)- C_4HS (6b**):** This complex was prepared as described for **6a**, from $\text{Bu}_3\text{SnC}\equiv\text{CH}$ (0.837 g, 2.55 mmol), 2,5-diiodo-3-butylthiophene (0.500 g, 1.28 mmol) and $\text{Pd}(\text{PPh}_3)_4$ (30 mg, 0.03 mmol) in dioxane (30 mL), LDA (1.5 mL, 2 M) and ($\eta^5\text{-C}_5\text{H}_5$) $\text{Fe}(\text{CO})_2\text{I}$ (0.799 g, 2.55 mmol). Step 3 was accomplished by stirring at 70 °C for 10 h. After repeated precipitation cycles from CH_2Cl_2 /pentane the product (0.352 g, 51% yield) was recovered as described for **6a** as a coffee-brown powder. IR (CH_2Cl_2): 2095 (w) $\tilde{\nu}_{\text{C}=\text{C}}$, 2042 (s), 1997 (s) $\tilde{\nu}_{\text{CO}}$ cm^{-1} . ^1H NMR (C_6D_6): δ = 7.73 (thioph.), 4.04 (Cp), 2.85, 1.70–0.80 (C_4H_9) ppm. ^{13}C NMR ($[\text{D}_7]\text{DMF}$): δ = 213.2, 141.9, 131.3, 128.4, 107.3, 89.5, 85.9, 71.7, 66.3, 31.8, 21.7, 13.1 ppm. $\text{C}_{26}\text{H}_{20}\text{Fe}_2\text{O}_4\text{S}$ (540.20): calcd. C 57.81, H 3.73; found C 57.60, H 3.83.

2,5-Bis[($\eta^5\text{-C}_5\text{H}_5$) $\text{Fe}(\text{CO})_2(\sigma^1\text{-C}\equiv\text{C})$]-3-($\text{C}_{16}\text{H}_{33}$)- C_4HS (6c**):** This complex was prepared as described for **6a**, from $\text{Bu}_3\text{SnC}\equiv\text{CH}$ (0.586 g, 1.79 mmol), 2,5-diiodo-3-hexadecylthiophene (0.500 g, 0.89 mmol) and $\text{Pd}(\text{PPh}_3)_4$ (16 mg, 0.01 mmol) in dioxane (30 mL), LDA (1.1 mL, 2 M) and ($\eta^5\text{-C}_5\text{H}_5$) $\text{Fe}(\text{CO})_2\text{I}$ (0.559 g, 1.78 mmol). Step 3 was accomplished by stirring at 65 °C for 23 h. After repeated precipitation cycles from CH_2Cl_2 /methanol the product (0.09 g, 15% yield) was recovered as described for **6a** as a coffee-brown powder. IR (CH_2Cl_2): 2096 (w) $\tilde{\nu}_{\text{C}=\text{C}}$, 2042 (s), 1997 (s) $\tilde{\nu}_{\text{CO}}$ cm^{-1} . ^1H NMR (C_6D_6): δ = 7.52 (thioph.), 4.08 (Cp), 1.70–0.80 ($\text{C}_{16}\text{H}_{33}$) ppm. ^{13}C NMR (CDCl_3): δ = 249.6, 230.2, 158.8, 121.6, 90.6, 85.3, 31.9, 29.7, 29.4, 22.7, 22.3, 14.1 ppm. $\text{C}_{38}\text{H}_{44}\text{Fe}_2\text{O}_4\text{S}$ (708.52): calcd. C 64.42, H 6.26; found C 64.30, H 6.15.

1,4-Bis[($\eta^5\text{-C}_5\text{H}_5$) $\text{Fe}(\text{CO})_2(\sigma^1\text{-C}\equiv\text{C})$] C_6H_4 (6d**):** This complex was prepared as described for **6a**, from $\text{Bu}_3\text{SnC}\equiv\text{CH}$ (0.985 g, 3.00 mmol), 1,4-diiodobenzene (0.500 g, 1.5 mmol) and $\text{Pd}(\text{PPh}_3)_4$ (35 mg, 0.03 mmol) in dioxane (25 mL), LDA (1.8 mL, 2 M) and ($\eta^5\text{-C}_5\text{H}_5$) $\text{Fe}(\text{CO})_2\text{I}$ (0.940 g, 3.00 mmol). Step 3 was accomplished by stirring at 60 °C for 6 h. After repeated precipitation cycles from CH_2Cl_2 /pentane the product (0.406 g, 57% yield) was recovered as described for **6a** as a dark yellow powder. IR (CH_2Cl_2): 2107 (w) $\tilde{\nu}_{\text{C}=\text{C}}$, 2043 (s), 1996 (s) $\tilde{\nu}_{\text{CO}}$ cm^{-1} . ^1H NMR (C_6D_6): δ = 7.56 (benzene), 4.06 (Cp) ppm. ^{13}C NMR ($[\text{D}_7]\text{DMF}$): δ = 213.6, 131.7–124.9, 115.6, 91.1, 85.9 ppm. $\text{C}_{24}\text{H}_{14}\text{Fe}_2\text{O}_4$ (478.07): calcd. C 60.30, H 2.95; found C 60.53, H 2.91.

1,4-Bis[($\eta^5\text{-C}_5\text{H}_5$) $\text{Fe}(\text{CO})_2(\sigma^1\text{-C}\equiv\text{C})$]-2,5-bis(OC_4H_9) C_6H_2 (6e**):** This complex was prepared as described for **6a**, from $\text{Bu}_3\text{SnC}\equiv\text{CH}$ (0.692 g, 2.11 mmol), 1,4-diiodo-2,5-dibutoxybenzene (0.500 g, 1.05 mmol) and $\text{Pd}(\text{PPh}_3)_4$ (25 mg, 0.02 mmol) in dioxane (25 mL), LDA (1.3 mL, 2 M) and ($\eta^5\text{-C}_5\text{H}_5$) $\text{Fe}(\text{CO})_2\text{I}$ (0.661 g, 2.11 mmol). Step 3 was accomplished by stirring at 50 °C for 7 h. After repeated precipitation cycles from CH_2Cl_2 /hexane the product (0.320 g, 49% yield) was recovered as described for **6a** as a coffee-brown powder. IR (CH_2Cl_2): 2106 (w) $\tilde{\nu}_{\text{C}=\text{C}}$, 2041 (s), 1994 (s) $\tilde{\nu}_{\text{CO}}$ cm^{-1} . ^1H NMR (C_6D_6): δ = 7.72 (benzene), 4.19 (Cp), 3.75 (OCH_2), 1.62–0.92 [$\text{OCH}_2(\text{CH}_2)_2\text{CH}_3$] ppm. ^{13}C NMR ($[\text{D}_7]\text{DMF}$): δ = 213.6, 130.4, 116.8, 86.5, 68.0, 19.1, 13.3 ppm. $\text{C}_{32}\text{H}_{30}\text{Fe}_2\text{O}_6$ (622.28): calcd. C 61.77, H 4.86; found C 61.90, H 4.81.

1,4-Bis[($\eta^5\text{-C}_5\text{H}_5$) $\text{Fe}(\text{CO})_2(\sigma^1\text{-C}\equiv\text{C})$]-2,5-bis(OC_8H_{17}) C_6H_2 (6f**):** This complex was prepared as described for **6a**, from $\text{Bu}_3\text{SnC}\equiv\text{CH}$ (0.896 g, 2.73 mmol), 1,4-diiodo-2,5-dioctyloxybenzene (0.800 g, 1.36 mmol) and $\text{Pd}(\text{PPh}_3)_4$ (32 mg, 0.03 mmol) in dioxane (25 mL),

LDA (1.7 mL, 2 M) and $(\eta^5\text{-C}_5\text{H}_5)\text{Fe}(\text{CO})_2\text{I}$ (0.855 g, 2.73 mmol). Step 3 was accomplished by stirring at 80 °C for 12 h. After repeated precipitation cycles from CH_2Cl_2 /methanol the product (0.521 g, 52% yield) was recovered as described for **6a** as a brown powder. IR (CH_2Cl_2): 2106 (w) $\tilde{\nu}_{\text{C}=\text{C}}$, 2042 (s), 1996 (s) $\tilde{\nu}_{\text{CO}}$ cm^{-1} . ^1H NMR (C_6D_6): δ = 4.20 (Cp), 3.70 (OCH₂), 1.50–0.90 [OCH₂(CH₂)₆CH₃] ppm. ^{13}C NMR (CDCl_3): δ = 212.5, 154.0–110.0, 85.4, 69.2, 29.4–22.6, 14.1 ppm. $\text{C}_{40}\text{H}_{46}\text{Fe}_2\text{O}_6$ (734.50): calcd. C 65.41, H 6.31; found C 65.32, H 6.27.

4,4'-Bis[($\eta^5\text{-C}_5\text{H}_5$)Fe(CO)₂($\sigma^1\text{-C}\equiv\text{C}$)](C₆H₄)₂ (6g**):** This complex was prepared as described for **6a**, from $\text{Bu}_3\text{SnC}\equiv\text{CH}$ (1.031 g, 3.14 mmol), 4,4'-dibromobiphenyl (0.500 g, 1.57 mmol) and Pd(PPh₃)₄ (37 mg, 0.03 mmol) in dioxane (30 mL), LDA (1.9 mL, 2 M) and $(\eta^5\text{-C}_5\text{H}_5)\text{Fe}(\text{CO})_2\text{I}$ (0.984 g, 3.14 mmol). Step 3 was accomplished by stirring at 80 °C for 9 h. After repeated precipitation cycles from CH_2Cl_2 /pentane the product (0.728 g, 84% yield) was recovered as described for **6a** as a dark orange powder. IR (CH_2Cl_2): 2106 (w) $\tilde{\nu}_{\text{C}=\text{C}}$, 2041 (s), 1994 (s) $\tilde{\nu}_{\text{CO}}$ cm^{-1} . ^1H NMR (C_6D_6): δ = 7.66–7.01 (biph), 4.10 (Cp) ppm. ^{13}C NMR ([D₇]-DMF): δ = 213.6, 136.2–125.5, 115.3, 92.5, 86.0 ppm. $\text{C}_{30}\text{H}_{18}\text{Fe}_2\text{O}_4$ (554.16): calcd. C 65.02, H 3.27; found C 65.15, H 3.29.

2,5-Bis[($\eta^5\text{-C}_5\text{H}_5$)Fe(dppe)($\sigma^1\text{-C}\equiv\text{C}$)]C₄H₂S (7a**):** A rust colour mixture of 2,5-bis[($\eta^5\text{-C}_5\text{H}_5$)Fe(CO)₂($\sigma^1\text{-C}\equiv\text{C}$)]C₄H₂S (**6a**) (0.247 g, 0.51 mmol) and 1,2-bis(diphenylphosphanyl)ethane (0.406 g, 1.02 mmol) in benzene (200 mL) was exposed to ultraviolet irradiation for 2 h at room temperature. The dark brown reaction mixture was then filtered and dried under vacuum. The black residue was washed with hexane, dissolved in toluene and precipitated with hexane. This treatment was repeated three times to isolate a crystalline black powder (0.137 g, 23% yield). IR (CH_2Cl_2): 2052 (w) $\tilde{\nu}_{\text{C}=\text{C}}$ cm^{-1} . ^1H NMR (C_6D_6): δ = 7.96, 7.40–6.90, 4.21 (Cp), 2.50–0.40 ppm. ^{13}C NMR (C_6D_6): δ = 142.7–128.0, 114.2, 99.7, 81.7, 30.2, 28.6 ppm. ^{31}P NMR (C_6D_6): δ = 106.9 ppm. $\text{C}_{70}\text{H}_{60}\text{Fe}_2\text{P}_4\text{S}$ (1168.90): calcd. C 71.93, H 5.17; found C 72.05, H 5.09.

1,4-Bis[($\eta^5\text{-C}_5\text{H}_5$)Fe(dppe)($\sigma^1\text{-C}\equiv\text{C}$)]C₆H₄ (7d**):** A yellow-orange mixture of 1,4-bis[($\eta^5\text{-C}_5\text{H}_5$)Fe(CO)₂($\sigma^1\text{-C}\equiv\text{C}$)]C₆H₄ (**6d**) (0.200 g, 0.42 mmol) and 1,2-bis(diphenylphosphanyl)ethane (0.345 g, 0.42 mmol) in benzene (200 mL) was exposed to ultraviolet irradiation for 3.5 h at room temperature. The dark red reaction mixture was then filtered and dried under vacuum. The residue was washed with hexane, dissolved in toluene and precipitated with hexane. This treatment was repeated ten times, and the pure complex (0.056 g, 12% yield) was finally recovered as a crystalline black powder. IR (CH_2Cl_2): 2065 (w) $\tilde{\nu}_{\text{C}=\text{C}}$ cm^{-1} . ^1H NMR (C_6D_6): δ = 7.98, 7.69, 6.99, 4.28 (Cp), 2.68–0.90 ppm. ^{31}P NMR (C_6D_6): δ = 107.1 ppm. $\text{C}_{72}\text{H}_{62}\text{Fe}_2\text{P}_4$ (1162.87): calcd. C 74.37, H 5.37; found C 74.64, H 5.81.

4,4'-Bis[($\eta^5\text{-C}_5\text{H}_5$)Fe(dppe)($\sigma^1\text{-C}\equiv\text{C}$)](C₆H₄)₂ (7g**):** A brick-red mixture of 4,4'-bis[($\eta^5\text{-C}_5\text{H}_5$)Fe(CO)₂($\sigma^1\text{-C}\equiv\text{C}$)](C₆H₄)₂ (**6d**) (0.150 g, 0.26 mmol) and 1,2-bis(diphenylphosphanyl)ethane (0.222 g, 0.54 mmol) in benzene (200 mL) was exposed to ultraviolet irradiation for 2 h at room temperature. The yellow-orange reaction mixture was then filtered and dried under vacuum. The light-orange residue was washed with hexane, dissolved in toluene and precipitated with hexane. This treatment was repeated ten times, and the pure product (0.060 g, 19% yield) was finally recovered as a dark yellow powder. IR (CH_2Cl_2): 2059 (w) $\tilde{\nu}_{\text{C}=\text{C}}$ cm^{-1} . ^1H NMR (C_6D_6): δ = 8.01, 7.25–6.90, 4.30 (Cp), 2.57–0.43 ppm. ^{13}C NMR ([D₇]-DMF, ppm): δ = 133.5–120.3, 105.2, 84.8, 78.6, 66.9, 29.9 ppm. ^{31}P NMR (C_6D_6): δ = 107.1 ppm. $\text{C}_{78}\text{H}_{66}\text{Fe}_2\text{P}_4$ (1238.97): calcd. C 75.62, H 5.37; found C 75.40, H 5.11.

[[Fe($\eta^5\text{-C}_5\text{H}_5$)($\eta^2\text{-dppe}$)(C $\equiv\text{C}$)₂]{2,5-C₄H₂S}][BF₄] (7a**⁺):** [Fe($\eta^5\text{-C}_5\text{Me}_5$)₂][BF₄] (0.0033 g, 0.0081 mmol, 0.95 equiv.) was added at room temperature to a stirred solution of [[Fe($\eta^5\text{-C}_5\text{H}_5$)($\eta^2\text{-dppe}$)(C $\equiv\text{C}$)₂]{2,5-C₄H₂S}] (**7a**) (0.01 g, 0.0085 mmol) in CH_2Cl_2 (10 mL). The wine-coloured mixture immediately became blue and was stirred at room temperature for 1.5 h. The solution was filtered through Celite, reduced in vacuo to about 2 mL, and hexane (15 mL) was added, allowing precipitation of a blue solid. After decantation of supernatant pale yellow liquid, the precipitate was washed several times with 5 mL of hexane, and dried under vacuum yielding the pure [[Fe($\eta^5\text{-C}_5\text{H}_5$)($\eta^2\text{-dppe}$)(C $\equiv\text{C}$)₂]{2,5-C₄H₂S}][BF₄] as blue microcrystals (0.0102 g, 95%). IR (CH_2Cl_2): 2059 (s) $\tilde{\nu}_{\text{C}=\text{C}}$ cm^{-1} . $\text{C}_{70}\text{H}_{60}\text{BF}_4\text{Fe}_2\text{P}_4\text{S}$ (1255.70): calcd. C 66.96, H 4.82; found C 66.64, H 4.63.

Computational Details: Full geometry optimisations with tight conditions were performed at B3LYP level of theory, as implemented in Gaussian03.^[21] The hybrid functional is Becke's three-parameter nonlocal exchange functional^[22] with the local correlation functional of Lee, Yang and Parr et al.^[23] The choice of this functional is motivated by the successful results obtained in geometry calculations of both neutral and charged similar complexes^[7p] and by its performance reported in very recent studies on the electronic coupling in mixed-valence organometallic complexes.^[20a,24] In both spin-restricted and spin-unrestricted calculations the 6-31G** basis set was used for S, P, O, C and H and the standard LANL2DZ-ECP was employed for Fe (B3LYP/LANL2DZ, 6-31G**).^[25] This choice is suitable for accurate results at an acceptable computational expenditure. In charged species the total spin values do not show significant spin contamination for doublet ion states. TDDFT excitation energies were calculated at B3LYP level of theory; standard LANL2DZ-ECP basis set was used for Fe and 6-31+G* was employed for all the other atoms (B3LYP/LANL2DZ, 6-31+G*⁺).^[25]

Supporting Information (see footnote on the first page of this article): UV/Vis spectra of **7a** and **7a**⁺; B3LYP/LANL2DZ,6-31G**-optimised geometries of the studied model complexes, and pictures of MOs involved in the NIR transitions.

Acknowledgments

This work was supported by the Consiglio Nazionale delle Ricerche (CNR, Roma) within the CNR/RAS (Russian Academy of Science, Moscow) bilateral agreement for financial support and by the Ministero dell'Istruzione, dell'Università e della Ricerca (MIUR) within the PRIN 2003 research project. We are grateful to Patrizia Gentili (Università "La Sapienza", Roma) for her very useful cooperation. CINECA (Consorzio Interuniversitario di Calcolo del Nord-Est, Casalecchio di Reno, Italia) is greatly acknowledged for the generous allocation of their computational facilities.

- [1] a) D. W. Bruce, D. O'Hare, *Inorganic Materials*, Wiley, Chichester, England, **1992**; b) Y. Sun, N. J. Taylor, A. J. Carty, *Organometallics* **1992**, *11*, 4293; c) D. L. Lichtenberger, S. K. Renshaw, A. Wong, C. Tagge, *Organometallics* **1993**, *12*, 3522; d) T. Bartik, B. Bartik, M. Brady, R. Dembinsky, J. A. Gladysz, *Angew. Chem. Int. Ed. Engl.* **1996**, *35*, 969; e) H. Lang, *Angew. Chem. Int. Ed. Engl.* **1994**, *33*, 547; f) U. H. F. Bunz, F. Beer, *Organometallics* **1995**, *14*, 2490; g) J. E. C. Wiegmann-Kreiter, U. H. F. Bunz, *Organometallics* **1995**, *14*, 4449; h) P. F. Schwab, M. D. Lewin, J. Michl, *Chem. Rev.* **1999**, *99*, 1863; i) T. Yamamoto, *Bull. Chem. Soc. Jpn.* **1999**, *72*, 621–638 and references cited therein; j) U. H. F. Bunz, *Chem. Rev.* **2000**, *100*, 1605–

- 1644; k) T. Yamamoto, *Synlett* **2003**, 4, 425; l) K. D. Demadis, C. M. Hartshorn, T. J. Meyer, *Chem. Rev.* **2001**, 101, 2655.
- [2] a) D. L. Zeckel, K. C. Hultsch, R. Rulken, D. Balaishis, Y. Ny, J. K. Pudelsky, A. J. Lough, I. Manners, D. A. Foucher, *Organometallics* **1996**, 15, 1972; b) M. J. Irwin, G. Jia, N. C. Payne, R. J. Puddenphatt, *Organometallics* **1996**, 15, 51; c) M. Altmann, U. H. F. Bunz, *Angew. Chem. Int. Ed. Engl.* **1995**, 34, 569; d) A. A. Dembeck, P. J. Fagan, M. Marsi, *Macromolecules* **1993**, 26, 2292; e) A. Kohler, H. F. Wittmann, R. H. Friend, M. S. Khan, J. Lewis, *Synth. Met.* **1996**, 77, 147; f) Y. Ni, R. Rulken, I. Manners, *J. Am. Chem. Soc.* **1996**, 118, 4102; g) G. Tomos, P. Nugara, M. V. Laksmikantham, M. P. Lava, *Synth. Met.* **1993**, 53, 271.
- [3] a) S. Takahashi, Y. Takai, H. Morimoto, K. Sonogashira, N. Hagihara, *Mol. Cryst. Liq. Cryst.* **1982**, 32, 139; b) D. Posselt, W. Badur, M. Steiner, M. Baumgarten, *Synth. Met.* **1993**, 55–57, 3299; c) M. Hmyene, A. Yassar, M. Escorne, A. Percheron-Guegan, F. Garnier, *Adv. Mater.* **1994**, 6, 564; d) W. L. Blau, H. J. Byrne, D. J. Cardin, A. P. Davey, *J. Mater. Chem.* **1991**, 1, 245; e) N. J. Long, *Angew. Chem. Int. Ed. Engl.* **1995**, 34, 21.
- [4] a) E. Antonelli, P. Rosi, C. Lo Sterzo, E. Viola, *J. Organomet. Chem.* **1999**, 578, 210; b) P. Altamura, G. Giardina, C. Lo Sterzo, M. V. Russo, *Organometallics* **2001**, 20, 4360; c) G. Giardina, P. Rosi, A. Ricci, C. Lo Sterzo, *J. Polym. Sci., Part A: Polym. Chem.* **2000**, 38, 2603; d) R. Pizzoferrato, M. Berliocchi, A. Di Carlo, P. Lugli, M. Venanzi, A. Micozzi, A. Ricci, C. Lo Sterzo, *Macromolecules* **2003**, 36, 2215; e) A. La Groia, A. Ricci, M. Bassetti, D. Masi, C. Bianchini, C. Lo Sterzo, *J. Organomet. Chem.* **2003**, 683, 406; f) A. Micozzi, M. Ottaviani, G. Giardina, A. Ricci, R. Pizzoferrato, T. Ziller, D. Compagnone, C. Lo Sterzo, *Adv. Synth. Catal.* **2005**, 347, 143.
- [5] a) E. Viola, C. Lo Sterzo, R. Crescenzi, G. Frachey, *J. Organomet. Chem.* **1995**, 493, C9–C13; b) E. Viola, C. Lo Sterzo, F. Trezzi, *Organometallics* **1996**, 15, 4352.
- [6] a) W. Beck, B. Niemer, M. Wieser, *Angew. Chem. Int. Ed. Engl.* **1993**, 32, 923; b) A. D. Hunter, *Organometallics* **1989**, 8, 118; c) E. A. Maatta, D. D. Devore, *Angew. Chem. Int. Ed. Engl.* **1988**, 27, 569; d) J. P. Collmann, J. T. McDevitt, C. R. Leidner, G. T. Yee, J. B. Torrance, W. A. Little, *J. Am. Chem. Soc.* **1987**, 109, 4606; e) S. J. Davis, B. F. J. Johnson, M. S. Fhan, J. Lawis, *J. Chem. Soc., Chem. Commun.* **1991**, 187; f) M. S. Khan, S. J. Davies, A. K. Kakkar, D. Schwartz, B. Lin, B. F. G. Johnson, J. Lewis, *J. Organomet. Chem.* **1992**, 424, 87; g) H. Fyfe, M. Mlekuz, D. Zargarian, N. J. Taylor, T. B. Marder, *J. Chem. Soc., Chem. Commun.* **1991**, 188; h) O. J. Stang, R. Tykwinsky, *J. Am. Chem. Soc.* **1992**, 114, 4411; i) J. Kiesewetter, G. Poingnant, V. Guerschais, *J. Organomet. Chem.* **2000**, 595, 81; j) T. L. Stott, M. O. Wolf, *Coord. Chem. Rev.* **2003**, 246, 89; k) O. Lavastre, M. Even, P. H. Dixneuf, A. Pacreau, J. P. Vairon, *Organometallics* **1996**, 15, 1530; l) M. C. B. Colbert, J. Lewis, N. J. Long, P. R. Raithby, M. Younus, A. J. P. White, D. J. Williams, N. N. Payne, L. Yellowlees, D. Beljonne, N. Chawdhury, R. H. Friend, *Organometallics* **1998**, 17, 3034; m) Y. Zhu, D. B. Millet, M. O. Wolf, S. J. Rettig, *Organometallics* **1999**, 18, 1930.
- [7] a) N. Le Narvor, C. Lapinte, *Organometallics* **1995**, 14, 634; b) N. Le Narvor, L. Toupet, C. Lapinte, *J. Am. Chem. Soc.* **1995**, 117, 7129; c) F. Coat, C. Lapinte, *Organometallics* **1996**, 15, 477; d) F. Coat, M. A. Guillevic, L. Toupet, F. Paul, C. Lapinte, *Organometallics* **1997**, 16, 5988; e) N. Le Narvor, C. Lapinte, *C. R. Acad. Sci., Ser. IIc: Chim.* **1998**, 745; f) M. Guillemot, L. Toupet, C. Lapinte, *Organometallics* **1998**, 17, 1928; g) T. Weyland, K. Costuas, A. Mari, J.-F. Halet, C. Lapinte, *Organometallics* **1998**, 17, 5569; h) S. Le Stang, F. Paul, C. Lapinte, *Organometallics* **2000**, 19, 1035–1043; i) F. Paul, W. E. Meyer, L. Toupet, H. Jiao, H. J. A. Gladysz, C. Lapinte, *J. Am. Chem. Soc.* **2000**, 122, 9405; j) R. Denis, L. Toupet, F. Paul, C. Lapinte, *Organometallics* **2000**, 19, 4240; k) T. Weyland, K. Costuas, L. Toupet, J.-F. Halet, C. Lapinte, *Organometallics* **2000**, 19, 4228; l) T. Weyland, I. Ledoux, S. Brasselet, J. Zyss, C. Lapinte, *Organometallics* **2000**, 19, 5235; m) H. Jiao, K. Costuas, J. A. Gladysz, J.-F. Halet, M. Guillemot, L. Toupet, F. Paul, C. Lapinte, *J. Am. Chem. Soc.* **2003**, 125, 9511; n) J. Courmarcel, G. Le Gland, L. Toupet, F. Paul, C. Lapinte, *J. Organomet. Chem.* **2003**, 670, 108; o) T. Weyland, C. Lapinte, G. Frapper, M. J. Calhorda, J.-F. Halet, L. Toupet, *Organometallics* **1997**, 16, 2024; p) K. M.-C. Wong, S. C.-F. Lam, C.-C. Ko, N. Zhu, V. W.-W. Yam, S. Roué, C. Lapinte, S. Fathallah, K. Costuas, S. Kahlal, J.-F. Halet, *Inorg. Chem.* **2003**, 42, 7086; q) K. Costuas, F. Paul, L. Toupet, J.-F. Halet, C. Lapinte, *Organometallics* **2004**, 23, 2053; r) S. Roué, C. Lapinte, T. Bataille, *Organometallics* **2004**, 23, 2558; s) F. de Montigny, G. Argouarch, K. Costuas, J.-F. Halet, T. Roisnel, L. Toupet, C. Lapinte, *Organometallics* **2005**, 24, 4558; t) M. I. Bruce, K. Costuas, T. Davin, B. G. Ellis, J.-F. Halet, C. Lapinte, P. J. Low, M. E. Smith, B. W. Skelton, L. Toupet, A. H. White, *Organometallics* **2005**, 24, 3864; u) F. de Montigny, G. Argouarch, K. Costuas, J.-F. Halet, T. Roisnel, L. Toupet, C. Lapinte, *Organometallics* **2005**, 24, 4558.
- [8] a) M. Brady, W. Weng, Y. Zhou, J. W. Seyler, A. J. Amoroso, A. M. Arif, M. Böhme, G. Frenking, J. A. Gladysz, *J. Am. Chem. Soc.* **1997**, 119, 775; b) T. B. Peters, J. C. Bowling, A. M. Arif, J. A. Gladysz, *Organometallics* **1999**, 18, 3261; c) R. Dembinski, T. Bartik, B. Bartik, M. Jaeger, J. A. Gladysz, *J. Am. Chem. Soc.* **2000**, 122, 810; d) W. E. Meyer, A. J. Amoroso, C. R. Horn, M. Jaeger, J. A. Gladysz, *Organometallics* **2001**, 20, 1115; e) C. Herrmann, J. Neugebauer, J. A. Gladysz, M. Reiher, *Inorg. Chem.* **2005**, 44, 6174; f) F. Zhuravlev, J. A. Gladysz, *Chem. Eur. J.* **2004**, 10, 6510.
- [9] a) M. I. Bruce, L. I. Denisovich, P.-J. Low, S. M. Peregudova, N. A. Ustynyuk, *Mendeleev Commun.* **1996**, 200; b) M. I. Bruce, P. J. Low, K. Costuas, J.-F. Halet, S. P. Best, G. A. Heath, *J. Am. Chem. Soc.* **2000**, 122, 1949; c) M. I. Bruce, M. Ke, P. J. Low, B. W. Skelton, A. H. White, *Organometallics* **1998**, 17, 3539; d) M. I. Bruce, B. C. Hall, B. D. Kelly, P. J. Low, B. K. Skelton, A. H. White, *J. Chem. Soc., Dalton Trans.* **1999**, 3719; e) M. I. Bruce, P. Hinterding, E. R. T. Tiekink, B. W. Skelton, A. H. White, *J. Organomet. Chem.* **1993**, 450, 209.
- [10] a) M. B. Robin, P. Day, *Adv. Inorg. Chem. Radiochem.* **1967**, 10, 247; b) C. Creutz, H. Taube, *J. Am. Chem. Soc.* **1969**, 91, 3988; c) C. Creutz, *Prog. Inorg. Chem.* **1983**, 30, 1; d) D. E. Richardson, H. Taube, *Coord. Chem. Rev.* **1984**, 60, 107; e) R. J. Crutchley, *Adv. Inorg. Chem.* **1994**, 41, 273; f) M. D. Ward, *Chem. Soc. Rev.* **1995**, 24, 121; g) S. Barlow, D. O'Hare, *Chem. Rev.* **1997**, 97, 637; h) P. Chen, T. J. Meyer, *Chem. Rev.* **1998**, 98, 1439; i) F. Paul, C. Lapinte, *Coord. Chem. Rev.* **1998**, 178, 431; j) D. P. Arnold, G. A. Heath, D. A. James, *J. Porphyrins Phthalocyanines* **1999**, 3, 5; k) C. J. Atwood, W. E. Geiger, *J. Am. Chem. Soc.* **2000**, 122, 5477; l) A. Cecon, S. Santi, L. Orian, A. Bisello, *Coord. Chem. Rev.* **2004**, 248, 683; m) S. Santi, A. Cecon, F. Carli, L. Crociani, A. Bisello, M. Tiso, A. Venzo, *Organometallics* **2002**, 21, 2679; n) F. Barrière, N. Camire, W. E. Geiger, U. T. Mueller-Westerhoff, R. Sanders, *J. Am. Chem. Soc.* **2002**, 124, 7262.
- [11] a) J. K. Stille, *Angew. Chem. Int. Ed. Engl.* **1986**, 25, 508; b) T. N. Mitchell in *Metal-Catalyzed Cross-Coupling Reaction* (Eds.: F. Diederich, P. J. Stang), Wiley-VCH, Weinheim, Germany, **1988**; c) V. Farina, V. Krishnamurthy, W. J. Scott, *The Stille Reaction*, John Wiley & Sons, Inc., New York, **1998**.
- [12] R. B. King, L. W. Houk, K. H. Pannell, *Inorg. Chem.* **1969**, 8, 1042.
- [13] C. Lapinte, private communication.
- [14] a) G. C. Allen, N. S. Hush, *Prog. Inorg. Chem.* **1967**, 8, 357; b) N. S. Hush, *Prog. Inorg. Chem.* **1967**, 8, 391.
- [15] Z. Bao, Z. Y. Che, L. Yu, *Macromolecules* **1993**, 26, 5281.
- [16] R. G. Parr, W. Yang, *Density Functional Theory of Atoms and Molecules*, **1989**, Oxford University Press.
- [17] As previously described,^[70] the orientation of the FeCp(PH₃)₂ fragments relative to the plane of the aromatic core has a negligible influence on the structural and electronic features of these complexes. In a conformational study on PH₃-7a at the em-

- ployed level of theory we found no significant energy difference between the conformers, i.e., less than $0.3 \text{ kcal mol}^{-1}$. In addition, a full geometry optimisation was carried out on the model complex dHpe-7a (dHpe = $\text{PH}_2\text{CH}_2\text{CH}_2\text{PH}_2$) in order to investigate the effect of replacing a chelating ligand with two PH_3 ligands. The results, included in the Supporting Information, do not show a significant difference.
- [18] a) D. L. Lichtenberger, S. K. Renshaw, *Organometallics* **1993**, *12*, 3522; b) G. Frapper, M. Kertesz, *Inorg. Chem.* **1993**, *32*, 732; c) J. E. McGrady, T. Lovell, R. Stranger, M. G. Humphrey, *Organometallics* **1997**, *16*, 4004.
- [19] M. E. Casida, C. Jamorski, K. C. Casida, D. R. Salahub, *J. Chem. Phys.* **1998**, *108*, 4439.
- [20] a) F. A. Cotton, C. Y. Liu, C. A. Murillo, D. Villagran, X. Wang, *J. Am. Chem. Soc.* **2004**, *126*, 14822; b) C. E. Powell, M. P. Cifuentes, J. P. Morrall, R. Stranger, M. G. Humphrey, M. Samoc, B. Luther-Davies, G. A. Heath, *J. Am. Chem. Soc.* **2003**, *125*, 602; c) F. C. Grozema, L. P. Candeias, M. Swart, P. Th. van Duijnen, J. Wildeman, G. Hdziioanou, L. D. A. Siebbeles, J. M. Warman, *J. Chem. Phys.* **2002**, *117*, 11366; d) J. Cornil, D. Beljonne, J. L. Bredas, *J. Chem. Phys.* **1995**, *103*, 834.
- [21] M. J. Frisch, G. W. Trucks, H. B. Schlegel, G. E. Scuseria, M. A. Robb, J. R. Cheeseman, V. G. Zakrzewski, J. A. Montgomery Jr, R. E. Stratmann, J. C. Burant, S. Dapprich, J. M. Millam, A. D. Daniels, K. N. Kudin, M. C. Strain, O. Farkas, J. Tomasi, V. Barone, M. Cossi, R. Cammi, B. Mennucci, C. Pomelli, C. Adamo, S. Clifford, J. Ochterski, G. A. Petersson, P. Y. Ayala, Q. Cui, K. Morokuma, N. Rega, P. Salvador, J. J. Dannenberg, D. K. Malick, A. D. Rabuck, K. Raghavachari, J. B. Foresman, J. Cioslowski, J. V. Ortiz, A. G. Baboul, B. B. Stefanov, G. Liu, A. Liashenko, P. Piskorz, I. Komaromi, R. Gomperts, R. L. Martin, D. J. Fox, T. Keith, M. A. Al-Laham, C. Y. Peng, A. Nanayakkara, M. Challacombe, P. M. W. Gill, B. Johnson, W. Chen, M. W. Wong, J. L. Andres, C. Gonzalez, M. Head-Gordon, E. S. Replogle, J. A. Pople, *Gaussian03*, Revision A.11.3, Gaussian, Inc., Pittsburgh, PA, **2002**.
- [22] A. D. Becke, *Phys. Rev. A* **1988**, *38*, 3098.
- [23] C. Lee, W. Yang, R. G. Parr, *Phys. Rev. B* **1988**, *37*, 785.
- [24] M. Bühl, W. Thiel, *Inorg. Chem.* **2004**, *43*, 6377.
- [25] a) P. J. Hay, W. R. Wadt, *J. Chem. Phys.* **1985**, *82*, 270; b) P. J. Hay, W. R. Wadt, *J. Chem. Phys.* **1985**, *82*, 284; c) P. J. Hay, W. R. Wadt, *J. Chem. Phys.* **1985**, *82*, 299; d) Basis sets were obtained from the Extensible Computational Chemistry Environment Basis Set Database, Version 4/17/03, as developed and distributed by the Molecular Science Computing Facility, Environmental and Molecular Sciences Laboratory, which is part of the Pacific Northwest Laboratory, P.O. Box 999, Richland, WA 99352, USA, and funded by the US Department of Energy. The Pacific Northwest Laboratory is a multiprogram laboratory operated by the Battelle Memorial Institute for the US Department of Energy under contract DE-AC06-76RLO 1830.

Received: January 11, 2006
Published Online: May 2, 2006